DISCUSSION PAPER SERIES

DP13874

THE TERM STRUCTURE OF GOVERNMENT DEBT UNCERTAINTY

Antonio Mele, Yoshiki Obayashi and Shihao Yang

FINANCIAL ECONOMICS

ISSN 0265-8003

THE TERM STRUCTURE OF GOVERNMENT DEBT UNCERTAINTY

Antonio Mele, Yoshiki Obayashi and Shihao Yang

Discussion Paper DP13874
Published 19 July 2019
Submitted 15 July 2019

Centre for Economic Policy Research
33 Great Sutton Street, London EC1V 0DX, UK
Tel: +44 (0)20 7183 8801
www.cepr.org

THE TERM STRUCTURE OF GOVERNMENT DEBT UNCERTAINTY

Abstract

How valuable would it be to mitigate government debt volatility? This paper introduces a model that accounts for the complex structure of government bond volatility and provides predictions on the fair value of government bond variance swaps and derivatives referenced thereon. Our calibrated model predicts that expected volatilities frequently oscillate between episodes of backwardation and contango, a feature that is in stark contrast with dynamics observed in equity markets. We use the model in risk-management experiments and evaluate scenarios such as the reaction of the U.S. Treasury volatility curve to shocks including unanticipated Fed decisions or global economic imbalances. Unlike equity volatility dynamics, which may be specified exogenously without violating no-arbitrage conditions, government bond volatility must be consistent with the dynamics of the whole yield curve. The paper provides quasi-closed form solutions that can readily be implemented despite the high-dimensional no-arbitrage restrictions that underlie the model dynamics.

JEL Classification: G12, G13, E43, E44

Keywords: fixed income volatility, information content of government bond volatility, government bond variance swaps, Treasury markets

Antonio Mele - antonio.mele@usi.ch
Università della Svizzera Italiana and CEPR

Yoshiki Obayashi - yoshiki.obayashi@appliedacademics.com
Applied Academics, LLC

Shihao Yang - sean.shihao.yang@gmail.com
Harvard University

Acknowledgements
We wish to thank Mascia Bedendo, Peter Carr, Robert Engle, Fabio Mercurio and Neil Shephard for helpful discussions, and seminar participants at Frankfurt School of Management, Harvard Statistics Department seminar, NYU-Stern Volatility Institute, and Global Derivatives USA 2014 and FINEST 2017 Winter workshop at Università Cattolica for comments. The views and opinions expressed herein are those of the authors and do not necessarily reflect the views of Applied Academics, LLC.

The Term Structure of Government Debt Uncertainty*

Antonio Mele
Swiss Finance Institute, USI Lugano and CEPR

Yoshiki Obayashi
Applied Academics LLC

Shihao Yang
Harvard University

First draft: November 12, 2014. This version: July 12, 2019

Abstract

How valuable would it be to mitigate government debt volatility? This paper introduces a model that accounts for the complex structure of government bond volatility and provides predictions on the fair value of government bond variance swaps and derivatives referenced thereon. Our calibrated model predicts that expected volatilities frequently oscillate between episodes of backwardation and contango, a feature that is in stark contrast with dynamics observed in equity markets. We use the model in risk-management experiments and evaluate scenarios such as the reaction of the U.S. Treasury volatility curve to shocks including unanticipated Fed decisions or global economic imbalances. Unlike equity volatility dynamics, which may be specified exogenously without violating no-arbitrage conditions, government bond volatility must be consistent with the dynamics of the whole yield curve. The paper provides quasi-closed form solutions that can readily be implemented despite the high-dimensional no-arbitrage restrictions that underlie the model dynamics.

Keywords: fixed income volatility; information content of government bond volatility, government bond variance swaps; Treasury markets.

JEL: G12; G13; E43; E44.

*We wish to thank Mascia Bedendo, Peter Carr, Robert Engle, Fabio Mercurio and Neil Shephard for helpful discussions, and seminar participants at Frankfurt School of Management, Harvard Statistics Department seminar, NYU-Stern Volatility Institute, and Global Derivatives USA 2014 and FINEST 2017 Winter workshop at Università Cattolica for comments. The views and opinions expressed herein are those of the authors and do not necessarily reflect the views of Applied Academics, LLC.

1. Introduction

Two key milestones in modern asset pricing are the acknowledgment that capital market volatility is random (Engle, 2004) and that a specific portfolio of derivatives could be used to index and trade forward-looking measures of this volatility. While asset volatility is now understood as a distinct asset class, most of the insights into its measurement and pricing have been made in the equity space. In comparison, relatively little is known regarding indexing and pricing interest rate volatility. How do markets price uncertainty around interest rate movements? How does benchmarking work in the fixed income volatility space? How is asset evaluation affected in these markets by, or in anticipation of, tail events such as the Lehman's bankruptcy or Fed rate hikes? What type of derivative instruments would be able to mitigate losses arising from these events? This paper addresses these questions in relation to government bond markets. We consider a model with random government bond volatility and evaluate derivatives written on expected volatility. These derivatives provide valuable information regarding the term structure of expectations and the risk-premiums required to invest in these markets. Recent history provides us with an interesting laboratory where to test the predictions of our model.

Figure 1 plots the CBOE/CBOT 10-Year Treasury Note Volatility Index (TYVIX), calculated by Chicago Board Options Exchange since May 2013, which is the government bond counterpart to CBOE's popular VIX index for equity market volatility. Both indexes are linked to the fair value of variance swaps, which are contracts with payoffs based directly on the volatility of the underlying assets (see Section 2). In particular, in a government bond variance swap, one party purchases insurance from another for protecting against exposure to realized government bond volatility over a given horizon. To illustrate, the higher the expected uncertainty in Treasury markets in the next month, the higher TYVIX. Figure 1 reveals that, while the two indexes sometimes display similar dynamics, there are several episodes in which they exhibit divergent behavior. For example, TYVIX is more reactive than VIX to the initial phases of the 2008 subprime mortgage crisis. As a second example, during Spring 2009, good signals about the U.S. economy would trigger a reverse flight-to-quality: the ensuing bond sell-off and equity rally would lead VIX to decrease and TYVIX to spike. As a third example, the TYVIX almost doubles during the 2013 "taper tantrum," when the FED signaled the markets a tightening in its policy stance; in this same period, the VIX is range-bounded, seemingly unaffected by the events of the time.

These episodes suggest that fixed income volatility has economic content beyond that of equity volatility and deserves a distinct treatment. For example, a portfolio comprised of fixed income securities might not be adequately protected while only relying on VIX-related instruments. Moreover, fixed income volatility is likely to incorporate information on economic developments that is not captured by equity volatility. Finally, it has been known for long time that it would be problematic to price fixed income volatility only based on fixed income securities, due the incomplete nature of these markets (Collin-Dusfresne and Goldstein, 2002). Our model is calibrated to nearly fifteen years

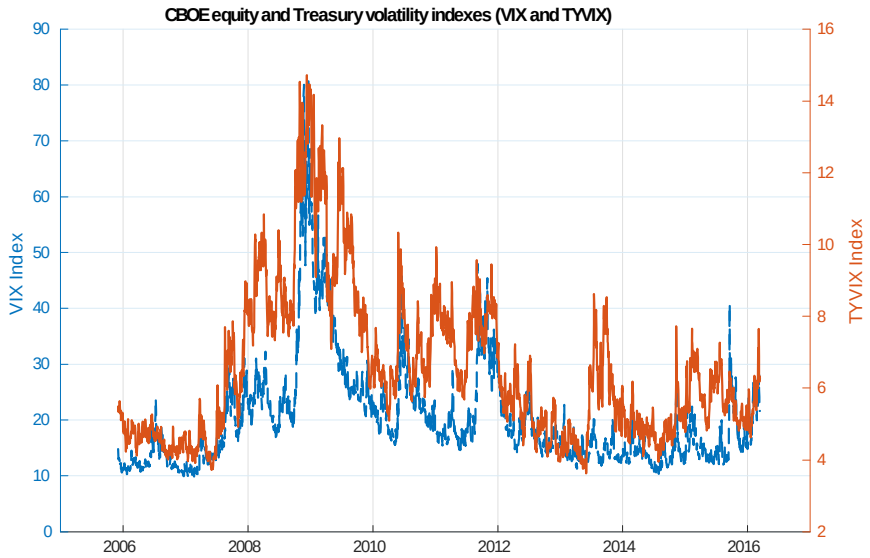

Figure 1. Indexes of equity and government bond volatility maintained by Chicago Board Options Exchange, VIX and TYVIX. Data are sampled daily and span the period from November 2005 to February 2016.

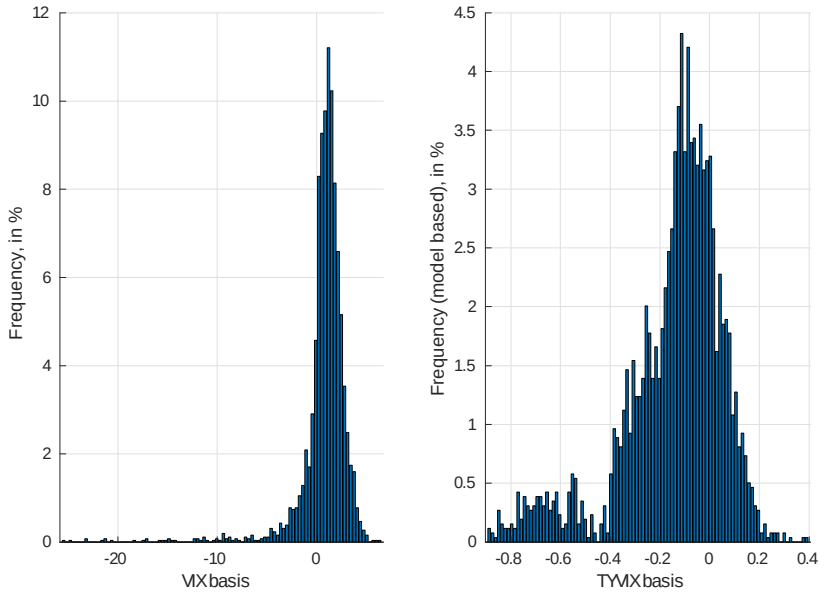

Figure 2. Frequency distribution of the basis in the equity and Treasury volatility spaces. *Left panel*: Distribution of the equity VIX basis, defined as the difference between 1-month future contracts and VIX levels. *Right panel*: Distribution of the Treasury VIX basis, defined as the difference between 1-month future contracts implied by the model of this paper and TYVIX levels. Data are sampled daily and span the period from November 2005 to February 2016.

of data to assess the potential role of derivatives on government bond volatility as both hedging instruments and sources of information. As we know, VIX is not investable, and the same is true of TYVIX. VIX futures and options are traded (and modeled). TYVIX futures have been introduced already while options have not yet. There are no models available to price derivatives on government bond volatility. Our model determines the value of these derivatives as well as that of the underlying expected volatility indexes. Due to the distinct nature of interest rate volatility, our problem needs a technical treatment that is separate from that available in the equity case.

While Figure 1 is instructive, equally important is the term structure of the price of uncertainty in both equity and fixed income markets. Future and option values provide valuable information regarding the market's expectation and aversion to the timing of uncertainty. A well-known feature of VIX is that its futures curve is often in contango: the VIX futures curve is increasing, perhaps reflecting risk aversion of the bid side of the market for volatility (see Figure 2). Our calibrated model implies that the U.S. Treasury market works quite differently: Figure 2 shows that our model predicts that TYVIX markets are more often in backwardation, i.e., they frequently come with an inverted future curve. A frequent backwardation is not an arbitrage opportunity, but it is puzzling, meaning as it does that insurance providers are not being paid for their role. The paper scope is bound to document this property, not to explain it. However, we use our model and investigate how this property may be exploited to help protect portfolios exposed to interest rate volatility. We provide evidence that overlaying fixed income portfolios with derivatives on government bond volatility may significantly mitigates the drawdowns occurring in such periods of acute volatility as those mentioned above. The model also helps understand episodes of historical importance such as the timing leading to volatility inversions vis-à-vis the increase in the FED rate targets in 2015, the reaction of the volatility curve to persistent or transitory shocks and, finally, the behavior of the "volatility of volatility," that is, the price of being insured against fluctuations in the volatility of Treasury markets throughout hypothetical options on TYVIX futures. We show that the volatility of volatility may help anticipate historically important episodes, such as the 2007 subprime crisis or the 2013 taper tantrum.

Our analysis relies on a model where the dynamics of the yield curve and volatility are driven by three factors: the short-term rate, its instantaneous volatility and a long-run uncertainty factor. We use this model to price government bond variance swaps and related derivatives. Mele and Obayashi (2015) provide a theoretical framework underlying the pricing of government bond variance swaps in a "model-free" fashion that does not hinge upon any assumptions other than absence of arbitrage and standard price dynamics based on Brownian motions. Our focus in this paper is on predicting government bond variance strikes and pricing derivatives based thereon, and relies on a parametric model. This approach is required whilst pricing derivatives on TYVIX: to evaluate contingent claims, we need to rely on a parametric model that describes random developments in the underlying risks.

Our model features two important properties. First, it accounts for the endogenous nature of government bond volatility, as explained below. Second, the model is formulated in a way that

variance swaps can be priced and hedged while ensuring that the entire yield curve is fitted without error. The second property is particularly appealing for the purpose of using the model consistent with the pricing of other securities, but also because it makes it possible for the entire current yield curve to feed information to the direction of future volatility.

An important feature of government bond price volatility is the presence of no-arbitrage restrictions it satisfies jointly with the underlying asset price. Intuitively, bond price volatility depends on the sensitivities of the bond price with respect to the variables that drive the whole yield curve. Because these sensitivities are endogenous, bond price volatility cannot be modeled separately from the underlying bond price. Equity volatility is more straightforward to model. For example, options written on stocks with stochastic volatility can be evaluated through arbitrary specifications of volatility, as the latter could be merely juxtaposed to the dynamics of stock returns for practical derivatives evaluation purposes (see, e.g., Heston, 1993).[1] Our model takes these features into account, and also provides quasi-closed form solutions that can be readily implemented to price futures and options on volatility indexes while also making sure that the underlying indexes are priced without errors.

The plan of the paper is as follows. The next section provides a succinct description of the framework behind government bond volatility: the dynamics of the underlying assets, the value of dedicated government bond variance swaps, and an index of forward-looking volatility arising therefrom. Sections 3 and 4 develop a parametric model of bond price volatility that leads to predictions on this government bond volatility index as well as the price of futures and options referenced to the index. Section 5 contains our empirical findings. Three Appendixes contain technical details omitted from the main text.

2. Government bond volatility: the underlying assets

2.1. Forward bond prices

Let $F_t(S,\mathbb{T})$ be the forward price at t, for delivery at S, of a coupon bearing bond expiring at $\mathbb{T}$, with $t \leq S \leq \mathbb{T}$. We assume the bond pays off coupons $\frac{C_i}{n}$ over the sequence of dates T_i, $i = 1, \cdots, N$, where n is the frequency of coupon payments, and $\mathbb{T} \equiv T_N$. The forward price satisfies $F_t(S,\mathbb{T}) = \frac{P_t^c(\mathbb{T})}{P_t(S)}$, where $P_t(S)$ is the price at t of a zero coupon bond expiring at $S \geq t$, $P_t^c(\mathbb{T})$ is the price at t of the underlying bond,

$$P_t^c(\mathbb{T}) \equiv \sum_{i=i_t}^{N} \frac{C_i}{n} P_t(T_i) + P_t(\mathbb{T}), \tag{1}$$

and T_{i_t} is the first available coupon payment date a bondholder would have access to.

Let r_t be the instantaneous short-term rate at time t and Q the risk-neutral probability. It is

[1] Models of equity evaluation relying on general equilibrium lead to a similar type of endogeneity though (see, e.g., Mele, 2007).

well-known[2] that in a diffusion setting, $F_t(S,\mathbb{T})$ satisfies

$$\frac{dF_\tau(S,\mathbb{T})}{F_\tau(S,\mathbb{T})} = v_\tau(S,\mathbb{T})\cdot dW_\tau^S, \quad \tau\in(t,S), \tag{2}$$

where $v_\tau(S,\mathbb{T})$ is the instantaneous volatility process adapted to W_τ^S, a multidimensional Brownian motion under Q_S (the S-forward probability), defined through the Radon-Nikodym derivative

$$\left.\frac{dQ_S}{dQ}\right|_{\mathbb{F}_S} = \frac{e^{-\int_t^S r_\tau d\tau}}{P_t(S)}, \tag{3}$$

and $\mathbb{F}_S$ denotes the information set at time S. Note that $v_\tau(S,\mathbb{T}) = \sigma_\tau^B(\mathbb{T}) - \sigma_\tau(S)$, where $\sigma_\tau^B(\mathbb{T})$ denotes the instantaneous volatility of the coupon bearing bond price, $P_t^c(\mathbb{T})$, and $\sigma_\tau(S)$ is the instantaneous volatility on a zero coupon bond expiring at S. We now describe the contracts that help investors hedge against fluctuations in the realized volatility of $P_t^c(\mathbb{T})$.

2.2. Government bond variance swaps

Consider the following payoff of a bond variance swap at time $T > t$

$$\pi(T,\mathbb{T}) \equiv V_t(T,S,\mathbb{T}) - \mathbb{P}(t,T,S,\mathbb{T}), \quad T\le S,$$

where $V_t(T,S,\mathbb{T}) \equiv \int_t^T \|v_\tau(S,\mathbb{T})\|^2 d\tau$ is the bond price integrated variance up to T, and $\mathbb{P}(t,T,\mathbb{T})$ is the variance swap strike. At inception, time-t, the value of this contract is zero, such that

$$\mathbb{P}(t,T,S,\mathbb{T}) = \frac{1}{P_t(T)}\mathbb{E}_t\left[e^{-\int_t^T r_\tau d\tau} V_t(T,S,\mathbb{T})\right] = \mathbb{E}_t^{Q_T}\left(V_t(T,S,\mathbb{T})\right), \tag{4}$$

where the second equality follows by a change of probability, and $\mathbb{E}_t$ and $\mathbb{E}_t^{Q_T}$ denote time-t conditional expectations under the risk-neutral probability and under the T-forward probability.

That is, the fair value of the variance swap is the expected realized variance under the T-forward probability. It is a notable point of departure from the standard equity case in which the fair value of a variance swap is the risk-neutral expectation assuming interest rates are constant. For the case at hand, we obviously cannot assume constant interest rates. Moreover, we still need to evaluate the R.H.S. of Eq. (4), which necessitates a theoretical treatment different from that leading to the standard equity VIX methodology.[3] This difference arises due to a "maturity mismatch": the expectation in Eq. (4) is taken under the T-forward probability, but the maturity of the forward price is $S \ge T$.

[2] See, e.g., Brigo and Mercurio (2006).

[3] See, e.g., Demeterfi, Derman, Kamal and Zou (1999,a,b), Bakshi and Madan (2000), Britten-Jones and Neuberger (2000), and Carr and Madan (2001).

Formally, the dynamics of $F_T(S,\mathbb{T})$ under the "variance swap" pricing probability are those under Q_T, not under Q_S as in Eq. (2), such that by Girsanov theorem,

$$\frac{dF_\tau(S,\mathbb{T})}{F_\tau(S,\mathbb{T})} = \underbrace{v_\tau(S,\mathbb{T})\left(v_\tau(S,\mathbb{T}) - v_\tau(T,\mathbb{T})\right)}_{\equiv z_\tau(T,S,\mathbb{T})} d\tau + v_\tau(S,\mathbb{T}) \cdot dW_\tau^T, \quad \tau \in (t,T), \tag{5}$$

where W_τ^T is a multidimensional Brownian motion defined under Q_T. The presence of a non-zero drift in Eq. (5) leads to a theoretical issue absent in the standard literature on equity variance swaps. In particular, Mele and Obayashi (2015) prove the following result:

Proposition 1. *The fair value of the variance swap in Eq. (4) is*

$$\begin{aligned}\mathbb{P}(t,T,S,\mathbb{T}) = {} & 2\left(1 - \mathbb{E}_t^{Q_T}\left(e^{\bar{z}(\tau,T,S,\mathbb{T})} - \bar{z}(t,T,S,\mathbb{T})\right)\right) \\ & + \frac{2}{P_t(T)}\left(\int_0^{F_t(S,\mathbb{T})} \mathrm{Put}_t(K)\frac{1}{K^2}dK + \int_{F_t(S,\mathbb{T})}^{\infty} \mathrm{Call}_t(K)\frac{1}{K^2}dK\right),\end{aligned} \tag{6}$$

where $\mathrm{Put}_t(K)$ *and* $\mathrm{Call}_t(K)$ *denote the prices of European puts and calls, written on bond forwards, struck at* K, $\bar{z}(t,T,S,\mathbb{T}) \equiv \int_t^T z_\tau(T,S,\mathbb{T})\,d\tau$, *and* $z_\tau(T,S,\mathbb{T})$ *is as in Eq. (5).*

A forward looking gauge of government bond volatility can then be based on the following index

$$\text{GB-VI}(t,T,S,\mathbb{T}) \equiv \sqrt{\frac{1}{T-t}\mathbb{P}(t,T,S,\mathbb{T})}, \tag{7}$$

where $\mathbb{P}(t,T,S,\mathbb{T})$ is as in Eq. (6).

Note that the first term in Eq. (6) is model-dependent: in general, the term $\bar{z}(t,T,S,\mathbb{T})$ is random and a model is needed to determine its expectation under Q_T. Even when $\bar{z}(t,T,S,\mathbb{T})$ is deterministic, we would need to estimate the volatilities $v_\tau(\cdot,\cdot)$ while at the same time relying on a model that ensures no arbitrage restrictions on the volatility curve, $v_\tau(\cdot,\cdot)$.

Eq. (B.11) in Appendix B provides the expression for $\bar{z}(t,T,S,\mathbb{T})$ predicted by the three-factor model with random volatility introduced in Section 3. Mele and Obayashi (2015, Chapter 4), rely on Vasicek's model (a special case of the model in Section 3), and document that, in practice, the contribution of the first term on the R.H.S. of Eq. (6) is very limited when $S-T$ is small. For example, Cboe Exchange Inc. (Cboe) maintains its TYVIX index relying on near- and next-month options on quarterly futures as underlying, which generates a negligible impact on $\mathbb{P}(t,T,S,\mathbb{T})$.

Note, finally, that the TYVIX index is calculated based on American options, not European. Mele and Obayashi (2015, Chapter 4) show that the presence of an early exercise premium might inflate the "true" index based on Eq. (7) by no more than one relative percentage point under realistic market conditions. We shall henceforth refer to the government bond volatility index in Eq. (7) as

TYVIX for conciseness.

3. A model of forward bond price volatility

In the equity literature, return volatility is modeled separately from the underlying stock returns (see, e.g., Mencía and Sentana, 2013), as explained in the Introduction. In contrast, government bond volatility cannot be taken to be exogenous. To illustrate, bond volatility converges to zero as time to maturity goes to zero, regardless of whether volatility is random. This and the following sections develop a model in which government bond volatility is determined endogenously, arising through no-arbitrage restrictions on bond price dynamics.

3.1. Fluctuating uncertainties and spot prices

We consider a market model: an extension of the Ho and Lee (1986) model, in which the short-term rate r_τ at any point in time $\tau \geq t$ is a mean-reverting process with mean-reverting stochastic volatility; and we also allow the *expected* short-term basis point variance to be time-varying, mean-reverting, and driven by an independent factor

$$\left\{\begin{array}{lcl} dr_\tau &=& \kappa_r\left(\theta_\tau - r_\tau\right)d\tau + v_\tau dW_{1\tau} \\ dv_\tau^2 &=& \kappa_v\left(\mu_\tau - v_\tau^2\right)d\tau + \xi v_\tau\left(\rho dW_{1\tau} + \sqrt{1-\rho^2}dW_{2\tau}\right) \\ d\mu_\tau &=& \kappa_\mu\left(m - \mu_\tau\right)d\tau + \gamma\sqrt{\mu_\tau}dW_{3\tau} \end{array}\right. \tag{8}$$

where W_j are standard Brownian motions under the risk-neutral probability. The standard approach to interest rate modeling is to assume that the short-term rate is mean-reverting around another mean-reverting long-term trend (see, e.g., Chapters 12-13 in Mele, 2019). In this model, basis point variance, v_τ^2, is mean-reverting around a long-term, mean-reverting uncertainty factor, μ_τ; finally, θ_τ is an "infinite dimensional" parameter that one may rely upon to fit the initial yield curve at the initial date t without errors. Remaining notation for the constant parameters should be straightforward. Note that we are assuming that the increments $d\mu_\tau$ are uncorrelated with dr_τ and dv_t^2: this assumption makes the model tractable, leading to exponential affine prices (see Proposition 2 below), which facilitates the modeling of variance contracts and the price of futures and options based thereon.

Preliminary empirical evidence gathered while calibrating a two-factor model (described in Appendix A) suggests that fluctuations in long-term interest rate uncertainty affect developments in near-term expected rate volatility. This preliminary evidence is at the basis of the formulation in (8), in which interest rate volatility fluctuates around a long-term uncertainty factor, μ_τ. Note that the assumption that volatility mean-reverts around a random term parallels similar assumptions made in the equity literature (e.g., Egloff, Leippold and Wu, 2010; Bates, 2012; Mencía and Sentana, 2013). The complication in this paper is that we price bond price volatility; while the latter is driven by both v_t^2 and μ_t, it also links, endogenously, to the elasticities of the bond price with respect to changes in

v_t^2 and μ_t, as we explain below.

We begin with summarizing the key properties of a zero coupon bond price predicted by the model.

Proposition 2. *If the short-term rate is solution to Eqs. (8), the price at $\tau \geq t$ of a zero coupon bond expiring at S when the state is $(r_\tau, v_\tau, \mu_\tau)$, is*

$$P_\tau\left(r_\tau, v_\tau^2, \mu_t, S\right) \equiv e^{A_S(\tau) - B_S(\tau) r_\tau + C_S(\tau) v_\tau^2 + D_S(\tau)\mu_\tau}, \tag{9}$$

for three functions $A_S(\cdot)$, $B_S(\cdot)$ and $C_S(\cdot)$ defined in Appendix B (see Eqs. (B.1), (B.2) and (B.3)).

Eq. (9) holds for any value taken by the time-varying parameter θ_τ (e.g., a constant); however, Appendix B provides the functional form for θ_τ (see Eq. (B.4)) such that the model predictions fit the initial yield curve without errors (see Eq. (B.5)). This feature allows us to make predictions regarding the future yield curve and, as discussed below, expected government bond volatility, while feeding the model with all the bond prices observed at time t, not only the short-term rate. It is standard market practice to allow a model for such a perfect fit (see, e.g., Mele and Obayashi, 2016), a procedure we have adapted to our environment with stochastic volatilities.

An interesting property of the model is that it allows the current yield curve to affect expected volatility. How is this property possible? Intuitively, the yield curve determines how future coupons are discounted, thereby affecting both the coupon bearing bond price and its volatility. For this reason, these "price feedbacks" only apply to coupon-bearing bonds, as explained next.

3.2. Forward prices and volatility

This section identifies the forward price volatility $v_\tau(S, \mathbb{T})$ in Eq. (2) predicted by the model of this section. Consider, first, the price of the forward on the coupon bearing bond; by Eq. (1), it is

$$F_t(S, \mathbb{T}) \equiv F_t\left(r_t, v_t^2, \mu_t, S, \mathbb{T}\right) \equiv \sum_{i=i_t}^{N} \frac{C_i}{n} F_t^z\left(r_t, v_t^2, \mu_t, S, T_i\right) + F_t^z\left(r_t, v_t^2, \mu_t, S, \mathbb{T}\right), \tag{10}$$

where

$$F_t^z(S, T_o) \equiv F_t^z\left(r_t, v_t^2, \mu_t, S, T_o\right) \equiv \frac{P_t\left(r_t, v_t^2, \mu_t, T_o\right)}{P_t\left(r_t, v_t^2, \mu_t, S\right)} \tag{11}$$

is the price of a forward expiring at $S \leq T_o$, written on a zero coupon bond expiring at some T_o, and $P_t\left(r_t, v_t^2, \mu_t, \cdot\right)$ is the price of a zero coupon bond predicted by Eq. (9). We now rely on Eqs. (10)-(11) and derive model-based predictions of volatility.

3.2.1. Zero coupon bonds

We first deal with zero coupon bonds. This case allows us to derive closed-form solutions for expected volatility, which we shall use in Section 3.2.2 while pricing the volatility of coupon bearing bonds. In Appendix B, we show that, under Q_T, the forward price in Eq. (11) is solution to

$$\left\{\begin{array}{lcl} \dfrac{dF_\tau^z(S,T_o)}{F_\tau^z(S,T_o)} & = & m_\tau^F d\tau + v_\tau\left(v_{1\tau}^z(S,T_o)\,dW_{1\tau}^T + v_{2\tau}^z(S,T_o)\,dW_{2\tau}^T\right) + \sqrt{\mu_\tau}v_{3\tau}^z(S,T_o)\,dW_{3\tau}^T \\ dv_\tau^2 & = & \left(\kappa_v\mu_\tau - G_T(\tau)\,v_\tau^2\right)d\tau + \xi v_\tau\left(\rho dW_{1\tau}^T + \sqrt{1-\rho^2}dW_{2\tau}^T\right) \\ d\mu_\tau & = & \left(\kappa_\mu m - H_T(\tau)\,\mu_\tau\right)d\tau + \gamma\sqrt{\mu_\tau}dW_{3\tau}^T \end{array}\right. \tag{12}$$

where the three volatility coefficients are, with $B.(\cdot)$, $C.(\cdot)$ and $D.(\cdot)$ defined as in Proposition 2,

$$\begin{array}{c} v_{i\tau}^z(S,T_o) = \varphi_{i\tau}(T_o) - \varphi_{i\tau}(S), \quad i=1,2,3, \\ \varphi_{1\tau}(\mathcal{X}) \equiv -B_{\mathcal{X}}(\tau) + \xi\rho C_{\mathcal{X}}(\tau), \quad \varphi_{2\tau}(\mathcal{X}) \equiv \xi\sqrt{1-\rho^2}C_{\mathcal{X}}(\tau), \quad \varphi_{3\tau}(\mathcal{X}) \equiv \gamma D_{\mathcal{X}}(\tau), \end{array} \tag{13}$$

and $G_T(\tau)$ and $H_T(\tau)$ are time-varying speeds of mean-reversion of the basis point variance v_τ^2 and long-term uncertainty μ_τ, and equal to

$$G_T(\tau) \equiv \kappa_v + \xi\left(\rho B_T(\tau) - \xi C_T(\tau)\right), \quad H_T(\tau) \equiv \kappa_\mu - \gamma^2 D_T(\tau), \quad \tau\in[t,T]. \tag{14}$$

Finally, Appendix B provides the expression for m_τ^F (see Eq. (B.6)).

With a slight abuse in notation, we define the volatility vector $v_\tau^z(v_\tau,\mu_t;S,T_o) \equiv [v_\tau^z(v_\tau;S,T_o) \quad \sqrt{\mu_\tau}v_{3\tau}^z(S,T_o)]$, where $v_\tau^z(v_\tau;S,T_o) = v_\tau \times [v_{1\tau}^z(S,T_o) \quad v_{2\tau}^z(S,T_o)]$. The next proposition provides an expression for the realized variance of a zero coupon bond price, and an ensuing forward looking volatility index.

Proposition 3. *Assume the short-term rate is solution to Eqs. (8). Then, the instantaneous realized variance of the forward price in Eqs. (12) is*

$$\|v_\tau^z(v_\tau,\mu_t;S,T_o)\|^2 = \phi_{1\tau}^z(S,T_o)\,v_\tau^2 + \phi_{2\tau}^z(S,T_o)\,\mu_\tau, \tag{15}$$

and the index of percentage volatility in Eq. (7) and, hence, the time t (square-root of the) fair value of a variance swap expiring at T, on a forward expiring at S, on a government zero coupon bond expiring at T_o is, for $t\le T\le S\le T_o$,

$$\text{GB-VI}^z\left(v_t^2,\mu_t;t,T,S,T_o\right) \equiv \sqrt{\kappa_m m\mathcal{B}_1^z(t,T,S,T_o) + \mathcal{B}_2^z(t,T,S,T_o)\,v_t^2 + \mathcal{B}_3^z(t,T,S,T_o)\,\mu_t}, \tag{16}$$

where $\phi_{j\tau}^z(S,T_o)$ are two deterministic functions of calendar time τ, and $\mathcal{B}_j^z(t,T,S,T_o)$ are three constants, all given in Appendix B (Eqs. (B.7) and (B.9)).

Eq. (15) tells us that the drivers of government bond *realized* variance are the short-term basis point variance v_τ^2 and the long-term uncertainty factor μ_τ. While the magnitude of v_τ^2 and μ_τ is too small to explain the level of realized government bond volatility, the two "multipliers" $\phi_{j\tau}^z(S,T_o)$ have the potential to increase this volatility by several orders of magnitude, depending on model parameters. In particular, Section 5 explains that there is compelling evidence that a "long-run risk" mechanism underlies these multipliers' effects: the higher the persistence of the short-term rate, its variance and long-term uncertainty, the higher the bond price exposures;[4] the higher these exposures, the higher the values of $\phi_{j\tau}^z(S,T_o)$. These magnifying effects operate in a nearly identical way on *expected* volatility, notably through the functions $\mathcal{B}_j^z(t,T,S,T_o)$ in Eq. (16). Naturally, these properties extend to the coupon bearing bond volatility case dealt with below. We shall return to these points in much more detail while discussing the model empirical implications (see Section 5).

Finally, note that the yield curve does not provide information regarding developments in government bond volatility: the government bond volatility index in Eq. (16) is independent of the yield curve at time-t. In contrast, we now show that the yield curve may well affect expected volatility of forwards on coupon bearing bonds.

3.2.2. Coupon bearing bonds and volatility feedbacks

By Eq. (10), the price of the forward on a coupon-bearing bond satisfies

$$\frac{dF_\tau(S,\mathbb{T})}{F_\tau(S,\mathbb{T})}=\sum_{i=i_t}^{N}\omega_\tau^i(S,\mathbb{T})\frac{dF_\tau^z(S,T_i)}{F_\tau^z(S,T_i)},\quad \omega_\tau^i(S,\mathbb{T})\equiv\bar{C}_i\frac{F_\tau^z(S,T_i)}{F_\tau(S,\mathbb{T})},\quad t<\tau<T<T_{i_t+1}, \tag{17}$$

where $\bar{C}_i\equiv\frac{C_i}{n}$ for $i=i_t,\cdots,N-1$, $\bar{C}_N\equiv\frac{C_N}{n}+1$, and $(C_i)_{i=1}^N$ denotes the series of coupons in Eq. (1).

In Appendix B, we provide the expression for the integrated drift that the model predicts for the forward price in Eq. (5).[5] Regarding the instantaneous realized variance of the forward price in Eq. (17), a direct calculation leaves

$$\left\|v_\tau(v_\tau,\mu_\tau;S,\mathbb{T})\right\|^2\equiv\left(\sum_{k=1}^{2}\left(\sum_{j=i_t}^{N}\omega_\tau^j(S,\mathbb{T})\,v_{k\tau}^z(S,T_j)\right)^2\right)v_\tau^2+\left(\sum_{j=i_t}^{N}\omega_\tau^j(S,\mathbb{T})\,v_{3\tau}^z(S,T_j)\right)^2\mu_\tau. \tag{18}$$

where $v_{k\tau}^z(S,T_j)$ are the zero coupon bond exposures in (13).

While summing up to one, the coupon bearing bond weights $\omega_\tau^j(S,\mathbb{T})$ are random, and therefore affect both current volatility and the whole future realized variance and its expectation under the forward probability. This feature of the model is a price feedback: the path of government bond volatility is driven by basis point variance and long-term uncertainty (v_τ^2 and μ_t), but also by the

[4] By Eq. (9), the bond price exposures are $B_S(\tau)$, $C_S(\tau)$ and $D_S(\tau)$.

[5] That is, $\bar{z}$ in Proposition 1; see Eq. (B.11).

entire yield curve, through the stochastic weights $\omega_\tau^j(S,\mathbb{T})$.

We wish to determine the fair value of a government bond variance swap based on the path of $\|v_\tau(v_\tau,\mu_\tau;S,\mathbb{T})\|^2$ and the ensuing government bond volatility index matching the TYVIX as described by Eq. (7). Because the weights $\omega_\tau^j(S,\mathbb{T})$ are random, closed-form solutions are not available that match Eq. (16) in Proposition 3. While Monte Carlo simulations could be used to approximate the model's predictions on TYVIX, this approach is computationally prohibitive, and becomes particularly so when the objective is to price derivatives on TYVIX on a large sample period (see Section 5). We rely on a different approximation: we replace the random weights $\omega_\tau^j(S,\mathbb{T})$ with their value taken at the evaluation time t, and proceed with pricing while relying on the "frozen" weights, $\omega_t^j(S,\mathbb{T})$.[6]

Let $y_t^\$(\tau) \equiv -\frac{1}{\tau}\ln P_t^\$(t+\tau)$ the yield at time t and maturity τ, where $P_t^\$(\cdot)$ is the observed counterpart zero to $P_t(\cdot)$, and let $\mathsf{Y}_{t,\mathbb{T}}^\$ \equiv \{y_t^\$(\tau)\}_{\tau\in(0,\mathbb{T}-t)}$ denote the entire yield curve observed at t and up to time to maturity $\mathbb{T}-t$. We have:

Proposition 4. *Assume the short-term rate is solution to Eqs. (8), and approximate $\omega_\tau^j(S,\mathbb{T})$ in Eq. (18) with $\omega_t^j(S,\mathbb{T})$. Then, the TYVIX index predicted by the model for time t, that is, the (square-root of the) fair value of a variance swap expiring at T, on a forward expiring at S, on a coupon bearing bond expiring at $\mathbb{T}$, is*

$$\text{GB-VI}(\mathsf{Y}_{t,\mathbb{T}}^\$, v_t^2, \mu_t; t, T, S, \mathbb{T}) = \sqrt{\kappa_\mu m \mathcal{B}_1(\mathsf{Y}_{t,\mathbb{T}}^\$, T, S, \mathbb{T}) + \mathcal{B}_2(\mathsf{Y}_{t,\mathbb{T}}^\$, T, S, \mathbb{T}) v_t^2 + \mathcal{B}_3(\mathsf{Y}_{t,\mathbb{T}}^\$, T, S, \mathbb{T})\mu_t}, \tag{19}$$

where $\mathcal{B}_i(Y_{t,\mathbb{T}}^\$,\cdot,\cdot,\cdot)$ are three functions given in Appendix B (see Eqs. (B.12)).

The model predicts that the government bond volatility index depends on the initial yield curve, $\mathsf{Y}_{t,\mathbb{T}}^\$$, because the instantaneous bond price realized variance $\|v_\tau(v_\tau,\mu_\tau;S,\mathbb{T})\|^2$ at τ depends on the coupon bearing bond weights $\omega_\tau^j(S,\mathbb{T})$ (see Eq. (18)) and, hence, the initial position of the yield curve. As explained, our approximation to the true government bond volatility index relies on freezing the weights $\omega_\tau^j(S,\mathbb{T})$ at $\omega_t^j(S,\mathbb{T})$.

4. Evaluation of government bond volatility derivatives

This section derives pricing implications regarding futures and options referenced to the TYVIX index predicted by the model (Eq. (19)). Section 5 explains that our calibration procedure is such that the model-based index exactly matches its empirical counterpart. As a byproduct of this matching, we obtain model-implied estimates of the unobservable realized variances v_t^2 and long-term uncertainties

[6] Similar approximations are utilized in the literature and market practice in other contexts. For example, these approximations are known as Rebonato's (1998) approximations in the context of the calculation of swaption volatilities (see, e.g., Brigo and Mercurio, 2006).

μ_t, which we reconstruct through Eq. (19). These estimates are used to feed the future and option pricing equations derived in this section.

4.1. Futures

The value at time t of a future contract, referenced to TYVIX, and expiring at time $t+\delta$, is

$$\mathcal{F}(\mathsf{Y}^{\$}_{t,\mathbb{T}}, v_t^2, \mu_t; t+\delta, T, S, \mathbb{T}) \equiv \mathbb{E}_t \left(\text{GB-VI}(\mathsf{Y}_{t+\delta,\mathbb{T}+\delta}, v_{t+\delta}^2, \mu_{t+\delta}; t+\delta, T+\delta, S+\delta, \mathbb{T}+\delta)\right), \tag{20}$$

where $\mathbb{E}_t$ denotes the expectation under the risk-neutral probability. The future value in Eq. (20) depends on the initial yield curve $\mathsf{Y}^{\$}_{t,\mathbb{T}}$ because the model prediction on the whole yield curve at $t+\delta$, $\mathsf{Y}_{t+\delta,\mathbb{T}+\delta}$, relies on the bond pricing model summarized by Proposition 2, and the latter pins down $\mathsf{Y}^{\$}_{t,\mathbb{T}}$ exactly while predicting $\mathsf{Y}_{t+\delta,\mathbb{T}+\delta}$. The yield curve at $t+\delta$ enters the TYVIX index predicted by the model through the weights $\omega^i_{t+\delta}(S+\delta, \mathbb{T}+\delta)$ in Eq. (17), as explained after Proposition 4.

Relying on Proposition 4, the future price in Eq. (20) is

$$\begin{aligned}&\mathcal{F}(\mathsf{Y}^{\$}_{t,\mathbb{T}}, v_t^2, \mu_t; t+\delta, T, S, \mathbb{T})\\ &= \iint \sqrt{\kappa_\mu m \mathcal{B}_1(\mathsf{Y}_{t_\delta,\mathbb{T}_\delta}, T_\delta, S_\delta, \mathbb{T}_\delta) + \mathcal{B}_2(\mathsf{Y}_{t_\delta,\mathbb{T}_\delta}, T_\delta, S_\delta, \mathbb{T}_\delta) v_{t+\delta}^2 + \mathcal{B}_3(\mathsf{Y}_{t_\delta,\mathbb{T}_\delta}, T_\delta, S_\delta, \mathbb{T}_\delta)\mu_{t+\delta}} \cdot \phi_t(x_{t+\delta}) dx_{t+\delta},\end{aligned} \tag{21}$$

where $\mathcal{B}_j(\mathsf{Y}_{t_\delta,\mathbb{T}_\delta}, T_\delta, S_\delta, \mathbb{T}_\delta) \equiv \mathcal{B}_j(\mathsf{Y}_{t+\delta,\mathbb{T}+\delta}, T+\delta, S+\delta, \mathbb{T}+\delta)$, $\phi_t(x')$ denotes the risk-neutral joint density of the state $x' \equiv (r', v^{2\prime}, \mu')$ conditional on (i) the initial yield curve, $\mathsf{Y}^{\$}_{t,\mathbb{T}}$, which includes the current short-term rate, r_t, and (ii) the basis point variance v_t^2 and long-run uncertainty μ_t.

Because the model in Eqs. (8) is affine, the joint density ϕ_t can be calculated in closed-form, up to the solution of a system of Riccati's equations.[7] However, the expression for $\mathcal{F}$ in Eq. (21) can be approximated by freezing the weights $\omega^j_{t+\delta}(S+\delta, \mathbb{T}+\delta)$ at $\omega^j_t(S, \mathbb{T})$, similarly as with the approximations leading to Eq. (19) of Proposition 4. Accordingly, the value at t of a TYVIX future maturing at $t+\delta$ can be approximated as

$$\begin{aligned}&\hat{\mathcal{F}}(\mathsf{Y}^{\$}_{t,\mathbb{T}}, v_t^2, \mu_t; t+\delta, T, S, \mathbb{T})\\ &\equiv \iint \sqrt{\kappa_\mu m \mathcal{B}_1(\mathsf{Y}^{\$}_{t,\mathbb{T}}, T, S, \mathbb{T}) + \mathcal{B}_2(\mathsf{Y}^{\$}_{t,\mathbb{T}}, T, S, \mathbb{T}) x + \mathcal{B}_3(\mathsf{Y}^{\$}_{t,\mathbb{T}}, T, S, \mathbb{T}) y} \cdot f_\delta\left(x, y | v_t^2, \mu_t\right) dxdy,\end{aligned} \tag{22}$$

where the transition density $f_\delta\left(x, y | v_t^2, \mu_t\right)$ is given in Appendix B (see Eq. (B.14)). This approximation considerably simplifies the numerical implementation of the model.

[7] Eqs. (8) have time-varying albeit deterministic parameters. The model is affine in that the conditional characteristic function can be shown to be exponential-affine in the state (r_t, v_t^2, μ_t), as in Duffie, Filipović and Schachermayer (2003).

4.2. Options

The pricing of options is slightly more elaborated than that of the futures because the relevant transition densities are needed under the forward probability, rather than the risk-neutral. Consider a European call option written on TYVIX, maturing at time $t+\Delta$, and struck at K. Its value is

$$\begin{aligned} & \mathcal{C}(\mathsf{Y}^{\$}_{t,\mathbb{T}}, v_t^2, \mu_t; t+\Delta, K, T, S, \mathbb{T}) \\ \equiv \;& P_t(T)\, \mathbb{E}_t^{Q_{t+\Delta}} \left(\text{GB-VI}(\mathsf{Y}_{t+\Delta,\mathbb{T}+\Delta}, v_{t+\Delta}^2, \mu_{t+\Delta}; t+\Delta, T+\Delta, S+\Delta, \mathbb{T}+\Delta) - K \right)^+ . \end{aligned} \quad (23)$$

Note that the expectation in Eq. (23) is now under the forward probability. Therefore, and similar to the futures evaluation (see Eq. (21)), the time t joint density of the state $(r_{t+\Delta}, v_{t+\Delta}^2, \mu_{t+\Delta})$ is needed to determine $\mathcal{C}$, albeit under the forward probability. It can be shown that (r_t, v_t^2, μ_t) is still an affine process under the forward probability, and so its conditional density is known in closed form, up to the solution of Riccati's equations. One approximation to Eq. (23) obtains while freezing the weights $\omega_{t+\Delta}^j(S+\Delta, \mathbb{T}+\Delta)$ at $\omega_t^j(S, \mathbb{T})$, similarly as with the futures evaluation equation (22). This yields the following approximation to the value at t of a TYVIX European call option maturing at $t+\Delta$ and struck at K:

$$\begin{aligned} & \hat{\mathcal{C}}(\mathsf{Y}^{\$}_{t,\mathbb{T}}, v_t^2, \mu_t; t+\Delta, K, T, S, \mathbb{T}) \equiv P_t(T) \\ & \times \iint \left(\sqrt{\kappa_\mu m \mathcal{B}_1(\mathsf{Y}^{\$}_{t,\mathbb{T}}, T, S, \mathbb{T}) + \mathcal{B}_2(\mathsf{Y}^{\$}_{t,\mathbb{T}}, T, S, \mathbb{T}) x + \mathcal{B}_3(\mathsf{Y}^{\$}_{t,\mathbb{T}}, T, S, \mathbb{T}) y} - K \right)^+ f_\Delta^F\left(x, y \middle| v_t^2, \mu_t\right) dxdy, \end{aligned} \quad (24)$$

where the transition density $f_\Delta^F\left(x, y \middle| v_t^2, \mu_t\right)$ is given in Appendix B (see Eq. (B.19)).[8]

While modeling options on TYVIX *levels* leads to the previous analytical solution, options on TYVIX *futures* are more likely candidates for listing. Options on futures can also be evaluated through a representation similar to Eq. (23). However, Section 5.2.4 explains that options on futures are computationally difficult to evaluate, and proposes an approximation scheme that is used to implement their pricing on our dataset. Eq. (24) is only provided for completeness.

5. Model predictions

We implement the model and reconstruct an hypothetical history of TYVIX futures and options values that could have traded on each day of our sample. We aim to shed light into a number of characteristics in this Treasury volatility market.

Firstly, we explore the main properties of TYVIX futures values in light of their trading implications: how would a long position in TYVIX futures drift over time? Secondly, we investigate the ability of TYVIX futures to hedge fixed income instruments: how would overlaying existing fixed

[8] Note that, in Section 5, we estimate the price of options written on TYVIX *futures*. For completeness, we provide Eq. (24), which regards option prices on TYVIX *levels*.

income portfolios help mitigate drawdowns during high volatility periods? Thirdly, we examine the model predictions in periods marked by tail events: how would the TYVIX futures curve react to an unanticipated monetary policy decision? Would this decision affect the whole futures curve? How would this reaction change following smaller shocks? Finally, we explore the behavior of hypothetical options values on TYVIX futures. We reconstruct TYVIX option values based on parameters calibrated to predict TYVIX futures, and analyze the behavior of this "volatility of volatility" during important historical events.

The next subsection succinctly describes the model calibration strategy, with technical details left in Appendix C. Our findings are in Section 5.2.

5.1. Calibration strategy

5.1.1. Data

The ideal situation to estimate our model would be one in which data could be available regarding both TYVIX and TYVIX derivatives (e.g., futures or options). Because futures on TYVIX were only launched in November 2014, our calibration relies on a proxy for the expected volatility in Treasury markets, namely at-the-money implied volatilities for CBOT's 10-year Treasury note options (TY options, for brevity); below, we shall explain how we use TY implied volatilities in our calibration procedure.

We use the three-month Treasury Bill rate as a proxy for the instantaneous interest rate r_t. Finally, note that our government bond volatility model also relies on market data for the yield curve up to the maturity of the underlying coupon-bearing bond;[9] therefore, our dataset also comprises the term structure of US government bonds up to the relevant maturities, which we take to equal $7\frac{1}{2}$ years, as further discussed below. Our sample, including TYVIX data, covers daily data available from Bloomberg from January 2, 2003 to February 19, 2016.

5.1.2. Risk-premiums

We assume that the basis point variance of the short-term rate has square root dynamics under the physical probability P, just as it does under the risk-neutral Q (see Eqs. (8)). Precisely, we assume that the Radon-Nikodym derivative of P against Q is

$$\left.\frac{dP}{dQ}\right|_{\mathbb{F}_T} = e^{-\frac{1}{2}\int_t^T \|\Lambda_\tau\|^2 d\tau - \int_t^T \Lambda_\tau dW_\tau^p},$$

where W_τ^p is a vector Brownian motion under P and, by Girsanov's theorem, its components satisfy: $dW_{i\tau}^p = dW_{i\tau} - \Lambda_{i\tau} d\tau$, with $\Lambda_{i\tau}$ denoting the i-th component of the risk-premium vector Λ_τ and, finally, $\Lambda_{i\tau} = \lambda_i^A v_\tau + \lambda_i^B \frac{1}{v_\tau}$ for $i = 1, 2$, and $\Lambda_{3\tau} = \lambda_3^A \sqrt{\mu_\tau} + \lambda_3^B \frac{1}{\sqrt{\mu_\tau}}$, for six constants $\left(\lambda_i^X\right)_{i\in\{1,2,3\};X\in\{A,B\}}$.

[9] That is, $\mathsf{Y}^{\$}_{t,\mathbb{T}}$ in Eqs. (19), (22) and (24); see also Eq. (31).

This specification of the risk-premiums makes the model "essentially affine" (Duffee, 2002). All in all, the coefficients λ_i^B accommodate the situation in which risk compensation relates to both the volatility of the state variables *and* some constant component; for example, compensation for the exposure to basis point volatility is $\Lambda_{2\tau} v_\tau = \lambda_2^A v_\tau^2 + \lambda_2^B$. Note that, based on assumptions made below, our calibration strategy does not necessitate making inference on any of the risk-premium coefficients. However, this discussion is instructive for the economic interpretation of our calibrated parameters.

Given our assumptions on risk-premiums, we have that under P, the basis point variance process v_τ^2 is solution to

$$dv_\tau^2 = \kappa_v^* \left(\mu_\tau^* - v_\tau^2\right) d\tau + \xi v_\tau \left(\rho dW_{1\tau}^p + \sqrt{1-\rho^2} dW_{2\tau}^p\right), \tag{25}$$

where

$$\kappa_v^* \equiv \kappa_v - \xi\lambda^A, \quad \mu_\tau^* \equiv \frac{\kappa_v}{\kappa_v^*}\mu_\tau + \frac{\xi}{\kappa_v^*}\lambda^B, \quad \lambda^X \equiv \rho\lambda_1^X + \sqrt{1-\rho^2}\lambda_2^X, \quad X \in \{A, B\}. \tag{26}$$

The (variance) persistence parameter under the physical probability P, κ_v^*, may differ from that under the risk-neutral Q, κ_v, namely due to λ^A; accordingly, we interpret λ^A as a "variance persistence risk-premium." Similarly, the "pull of attraction" of v_t^2 under P, μ_τ^*, may well have different dynamics under Q, due to risk-adjustments regarding both the short-term variance dynamics (λ^B in (26)) and its own long-term expected value (m^* below), i.e.,

$$d\mu_\tau^* = \kappa_\mu^* \left(m^* - \mu_\tau^*\right) d\tau + \gamma^* \sqrt{\mu_\tau^*} dW_{3\tau}^p, \tag{27}$$

where

$$\kappa_\mu^* \equiv \kappa_\mu - \gamma\lambda_3^A, \quad m^* \equiv \left(\frac{\kappa_\mu}{\kappa_\mu^*}m + \frac{\gamma}{\kappa_\mu^*}\lambda_3^B\right)\frac{\kappa_v}{\kappa_v^*} + \frac{\xi}{\kappa_v^*}\lambda^B, \quad \gamma^* \equiv \gamma\frac{\kappa_v}{\kappa_v^*}.$$

Accordingly, we interpret λ^B and λ_3^B as "long-run variance risk-premiums," and λ_3^A as a "long-term variance persistence risk-premium."

5.1.3. Model implementation

We calibrate the model using a sample period covering nearly fifteen years of daily data and we do then make a few simplifying assumptions. Namely, we assume that $\rho = 0$ and that the variance persistence risk-premiums are zero (i.e., $\lambda^A = \lambda_3^A = 0$), implying that $\kappa_v = \kappa_v^*$ and $\kappa_\mu \equiv \kappa_\mu^*$. We, then, create rolling window estimates $\hat{\sigma}_t^2$ (say) of the basis point variance v_t^2 of the short-term rate, relying on the 3-month Treasury Bill rate as a proxy of the short-term rate. We calibrate κ_v and ξ, by treating $\hat{\sigma}_t^2$ as it were the true basis point variance, and by matching the first and second moments of $\hat{\sigma}_t^2$ to the theoretical counterparts implied by the model. Table 1 reports our calibrated values for κ_v, annualized, and ξ. The parameters κ_μ and γ are calibrated similarly to κ_v and ξ, but are based on model-implied values of μ_t and we set m equal to the average value of the calibrated μ_t, as further

elaborated below.

Table 1. Calibrated parameter values and model-implied basis point uncertainties

κ_r	κ_v	ξ	avg (v^2)	avg (μ)	κ_μ	m	γ
0.0500	1.6057	0.0200	0.0132^2	0.0236^2	40.0235	0.0141^2	0.0759

We calibrate κ_r and μ to ensure that the model (i) matches the TYVIX without errors, (ii) fits the term structure of short positions in unhedged calendar spreads, a proxy for hypothetical futures values calculated on ATM option values, (iii) generates a basis point interest rate variance that has minimum distance from the sample average of $\hat{\sigma}_t^2$. The proxies for the futures values in (ii) are calculated throughout a non-parametric procedure known in the equity space since at least Carr and Wu (2006) and Dupire (2006): for the approximation to a future value as of day t and expiring on day $t+\delta$, we have

$$\mathcal{F}_t^{\$}(\delta) \equiv \sqrt{(\delta+1)\cdot \mathrm{atm}_t^2(\delta+1) - \delta \cdot \mathrm{atm}_t^2(\delta)}, \tag{28}$$

where $\mathrm{atm}_t(\delta)$ is the TY option ATM implied volatility for maturity δ (see Eq. (C.6) in Appendix C). Regarding the model prediction on TYVIX, we assume that the coupon bearing bond has time-to-maturity equal to $7\frac{1}{2}$ years and pays \$3 semi-annually; that is, in terms of Eq. (1), $C_i = \$6$, $n = 2$, and $\mathbb{T} - t = 7.5$.

We set m equal to the average estimates of long-run uncertainties, μ_t, obtained calibrating a two-factor version of the model in which μ_t is treated as a constant that is calibrated every day to produce minimum distance between the model-implied future values and the non-parametric estimates in Eq. (28) (see Eq. (C.4) in Appendix C). Finally, the parameter values in Table 1 are used to calibrate the three factor model-implied uncertainties v_t^2 and μ_t for each day, which then feed the model to produce predictions regarding future and option values.

Note that, in the model, m is the ergodic mean of both v_t^2 and μ_t under the risk-neutral probability Q. Precisely, and based on Eqs. (25) and (27), the ergodic means under the physical probability are $E_\infty^p\left(v_t^2\right) = m^*$ and $E_\infty^p(\mu_t) = m^* - \frac{\xi}{\kappa_v}\lambda^B$.[10] Given the average values of the model-implied times series of v_t^2 and μ_t in Table 1, we have the following estimates: $E_\infty^p\left(v_t^2\right) \approx 0.0132^2$ and $E_\infty^p(\mu_t) \approx 0.0236^2$; this situation is consistent with risk-premium coefficients satisfying $\lambda_3^B > 0$ and $\lambda^B < 0$.

Table 1 reports the parameter values for κ_r and summary statistics for the model-implied short-term variance v_t^2 and the model-implied expected basis point variance, μ_t. The model matches the data when the short-term rate under the risk-neutral probability is quite persistent, i.e., when κ_r is small. The main reason underlying this finding is that our model is calibrated over a sample period in which unprecedented monetary policy interventions occurred in response to the 2007-2009 global financial crisis, which kept both interest rates *and* interest rate volatility extraordinarily low. In this context, a persistent short-term rate helps our model predict relatively high values for risk-adjusted expected Treasury *volatility* on long-term bonds, acting as a risk for the "long run," in analogy with

[10] That is, for example, $E_\infty^p(\mu_t) \equiv \lim_{T\to\infty} E^p(\mu_T|\,\mu_0)$, where $E^p(\cdot|\,\cdot)$ denotes conditional expectation taken under the physical probability.

similar mechanisms put forward in the equity literature (see, e.g., Bansal and Yaron, 2004).

Note that the model-implied basis point realized variance (v_t^2 from Eq. (C.7) in Appendix C) is 0.0132^2 on average, which is higher than its statistical counterpart, $\text{avg}(\hat{\sigma}_t^2) = 0.0101^2$, i.e., an average volatility of about 100 basis points. Importantly, the model-implied realized basis point variance is on average only slightly lower than its long-term value under Q, i.e., the difference $m - \text{avg}(\hat{v}^2)$ is positive but small. This feature of the calibrated model leads to predictions of markets that are likely to experience frequent oscillations between contango and backwardation depending on the specific values taken by the realized short-term variance compared to its long-term risk-neutral expectation, m. This property leads to a variety of important implications, as we now explain.

5.2. Model implications

5.2.1. The calibrated futures term structure

The top panel of Figure 3 plots historical TYVIX levels against one-month futures prices based on the calibrated parameters and filtered values for both the short-term and long-term basis point variance, v_t^2 and μ_t. The two series track each other closely as one would reasonably expect for a short-dated futures price, while still exhibiting rich dynamics. For a closer examination of the difference, the bottom panel shows the future value minus the index level, or "TYVIX basis." It indicates that the market oscillates between contango and backwardation with sustained periods of backwardation. This observation stands in contrast to the analogous basis in equity markets, as measured by VIX and traded one-month VIX futures prices, which displays persistent contango during the same time period (see Figure 2 in the Introduction). In particular, our model suggests that hypothetical markets for TYVIX futures would have spent more time in backwardation than in contango, especially during the period 2007-2012.

The frequent backwardation is largely driven by the fact that we calibrate the model to fit the option-implied non-parametric estimate $\mathcal{F}_t^{\$}(\delta)$ in Eq. (28). By design, the model-implied one-month TYVIX futures closely track the non-parametric estimate based on ATM volatilities of TY options. This aspect of the calibration strategy is especially material when generating hypothetical historical futures prices as it imparts information on the volatility term structure from the TY options market to the shape of the estimated futures curve.[11]

Based on conversations with interest rate derivatives traders and strategists at numerous major dealer banks, the backwardation in the non-parametric estimates may be explained by the richness of the nearest month options that are often bid up going into scheduled macroeconomic announcements, such as non-farm payroll, GDP, and Federal Open Market Committee (FOMC) rate decisions.[12] Note that these features of the non-parametric estimates is *not* a possible artifact of how Bloomberg

[11] Section 5.2.3 provides more intuition regarding conditions under which the model leads to backwardation.

[12] We have conducted a separate event study of the behavior of TYVIX around major macroeconomic announcements, and found the results consistent with this anecdotal explanation. Our results are available upon request.

calculates generic one-month ATM implied volatilities for TY. Indeed, when options become extremely short-dated, e.g., within one week to expiry, traders cease to think in terms of implied volatilities and instead solely think in terms of prices because even one tick may correspond to large differences in implied volatilities. If the one-month implied volatilities are based in part on such short-dated options, it could then upwardly bias the one-month TY implied volatility data. However, Bloomberg does not use short-dated options while calculating implied volatilities in our dataset.

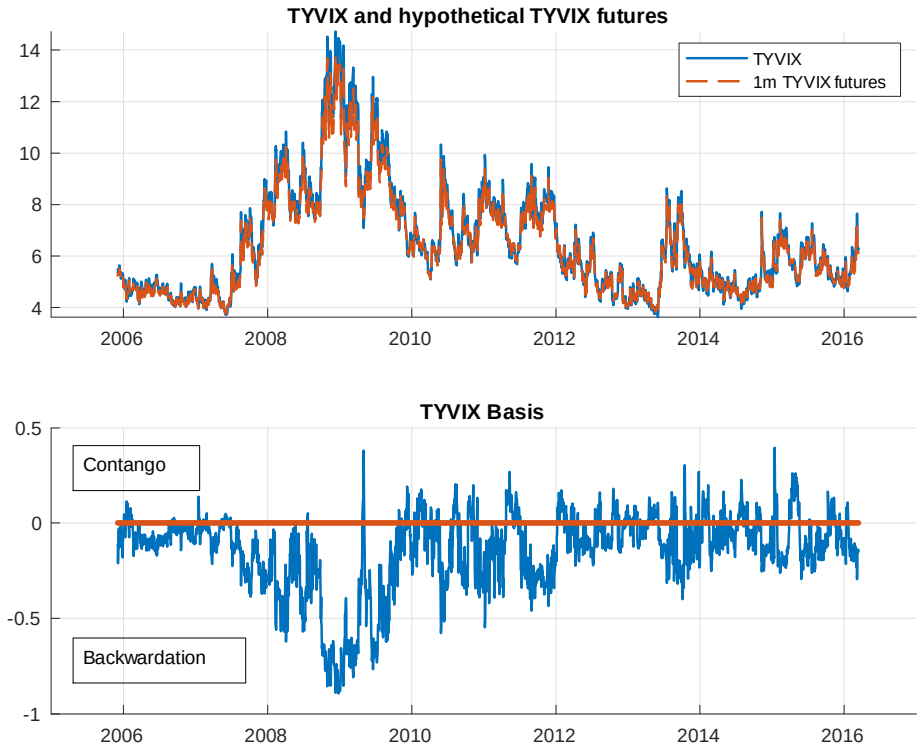

Figure 3. *Top panel*: CBOE-CBOT TYVIX index of Treasury volatility and model-based calibrated one month TYVIX futures. *Bottom panel*: TYVIX basis, defined as the difference between one month future values and TYVIX values.

The blue line in Figure 4 shows non-compounded cumulative returns from being long the TYVIX index as if one could trade the index like a stock. In practice, however, one cannot trade the index like a stock and futures do not have constant maturity. Assuming a monthly futures listing schedule, the green line shows non-compounded cumulative returns from always being long the nearest-month futures contract that has at least five days to expiry; similarly, the red line shows returns from being long the near- and next-month contracts with weights set such that the weighted time to maturity is always 21 trading days. There is a pronounced upward drift in the P&L for being constantly

long volatility using the simple rolling strategies, which is consistent with the frequent backwardation observed in Figure 3, and highlights the significant trading implications of the futures term structure.

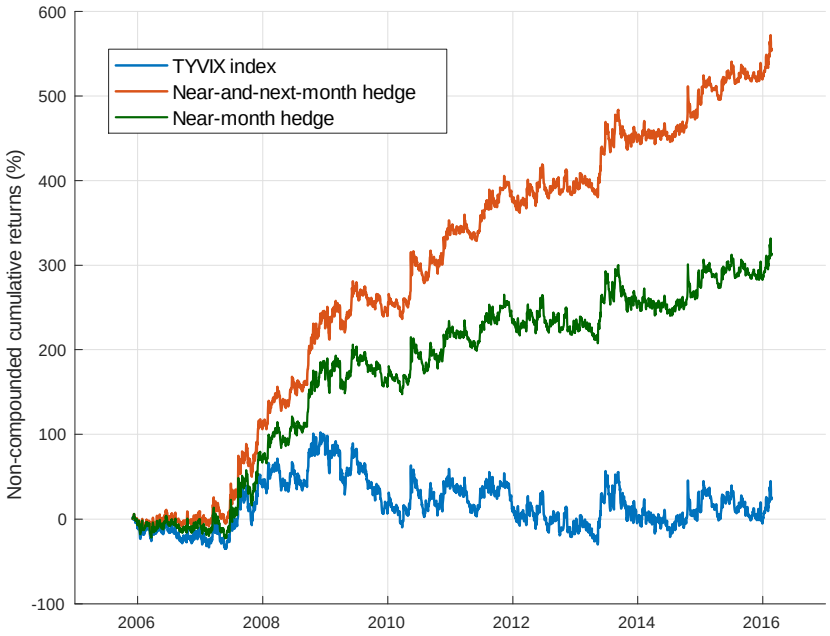

Figure 4. Cumulative returns from being long government bond volatility based on model-implied futures on the CBOE-CBOT TYVIX index of Treasury volatility. Red and green lines depict the P&L of strategies based on trading futures: the green is the P&L from holding the nearest-month future up to five days to expiry, and the red is the P&L from holding a portfolio of the near- and next-month futures with time-varying weights ensuring the average portfolio position is 21 trading days. The blue line tracks returns from being long the TYVIX as it was a tradeable asset.

Table 2 provides more precise details on this drifting properties of the rolling strategies, while zooming the period beginning from 2008. In this period, near-and-next month hedge strategies have comparable average returns, although the former have better performance, due to lower performance variability and lower drawdowns. Below, we use near-term strategies to hedge various ETFs both in the fixed income and the equity space.

Table 2. Performance of two volatility rolling strategies, the near-and-next and the near-month displayed in Figure 4. Mean and vol columns are the average returns and standard deviations of the investment strategies, annualized; Sharpe is the Sharpe ratio defined as the ratio of annualized means to standard deviations; Skewn. is the coefficient of skewness calculated on the strategies returns; Drawdn. is the maximum drawdown on the investment strategies. Sample period is from January 2, 2008 to February 19, 2016.

	Rolling strategies				
	mean	vol	Sharpe	Skewn.	Drawdn.
near-next	0.2169	0.2252	0.9634	1.5527	0.1814
near	0.2299	0.3415	0.6733	0.9587	0.2831

5.2.2. Applications to hedging bond portfolios

Given the prevalent use of equity volatility derivatives as equity portfolio hedging tools, a natural question that arises is whether interest rate volatility derivatives may be used for hedging bond portfolios. To address this question, we first examine the relation between returns on the near-term rolling hedging strategy explained in the previous section (the 21 day fixed maturity strategy depicted as the red line in Figure 4) and returns on the iShares Core U.S. Aggregate Bond ETF (ticker AGG), which is one of the most commonly-used diversified bond portfolio benchmarks.

Figure 5 shows adjusted-R^2 statistics from rolling OLS weekly regressions (and regression window equal to three years), with AGG returns are on the left-hand-side and the TYVIX log-changes on the right-hand side. We include analogous results for VIX for the sake of comparison. The plot reveals two spikes in the correlation between the bond portfolio and TYVIX futures that correspond to the US debt rating downgrade in 2011 and the "QE Taper Talk" in mid-2013; to the contrary, the correlation was nearly zero at the depth of the financial crisis. One interpretation is that bond portfolio performance and interest rate volatility become tighter linked when interest rate risk is a significant concern in the market; the correlation during the 2008-2009 period was low because interest rate risk did not play a key role in the crisis.

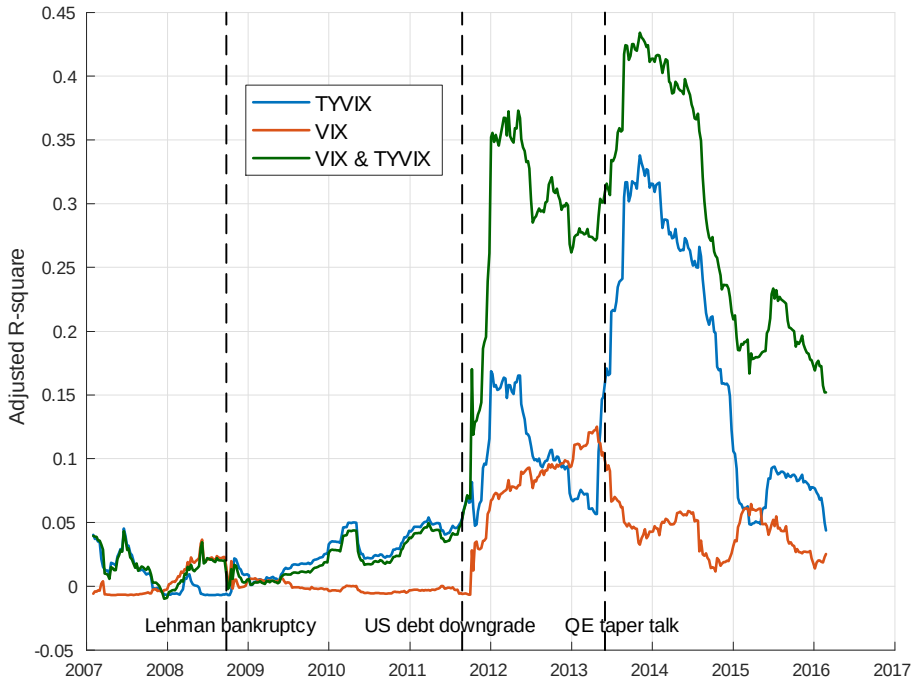

Figure 5. Adjusted-R^2 statistics calculated through weekly rolling regressions of the returns on the iShares Core U.S. Aggregate Bond ETF onto returns on model-implied one-month futures on TYVIX (blue line), returns on one-month futures on VIX (red), and returns on both TYVIX and VIX one-month futures (green). Estimation window is 3 years. One-month future returns on VIX and TYVIX are calculated through a portfolio of near- and next-month futures with time-varying weights ensuring the average portfolio position is 21 trading days (as in the TYVIX case depicted through the red line in Figure 4).

Naturally, TYVIX and VIX are not investable. For example, it is well-known that log changes in the VIX index cannot necessarily be replicated by log changes on traded VIX futures due to effects relating to the volatility term structure: the VIX future curve is in contango more often than not, as explained in the Introduction. Therefore, we re-calculate rolling regressions using AGG returns on the left-hand-side and the rolling near-term TYVIX futures strategy depicted in Figure 4 on the right-hand-side. We perform the same regressions relying on a similar rolling near-term VIX future strategy. Then, we overlay AGG returns based on the sign of the coefficient estimates in these regressions.

Figure 6 depicts unhedged and overlayed returns during the period comprising the QE Taper Talk events in 2013, from February 12, 2013 to February 18, 2014. The blue line shows the TYVIX hedged returns, which outperform the unhedged (in grey), by smoothing out two pronounced drawdowns.

Figure 6 shows that the VIX-hedged returns generally outperform the unhedged returns. The reason for this outperformance is that in this sampling period, VIX futures returns and AGG are positively correlated, and the hedging portfolio then prescribes selling VIX futures, which leads to monetizing a contango premium that is typical in VIX futures market. Note, however, that it would be quite unusual to protect a portfolio from spikes in market volatility while being short VIX futures. In fact, the VIX-hedged strategy is not as effective as the TYVIX-hedged strategy during the 2013 rate-driven events. Hedging AGG with VIX futures does lead indeed to one quite pronounced drawdown in this period.

The bottom panels of Figure 6 show how AGG returns are hedged reasonably well when we rely on both TYVIX and VIX rolling strategies, evidencing the role the TYVIX hedging strategy plays while insuring against rate-driven events. These very simple hedging results suggest that TYVIX futures may be an effective hedging tool for bond portfolios, given the tendency of implied volatilities to spike more than usual during pronounced bond market sell-offs.

Table 3 contains a quantitative assessment of our findings that relate to the whole sampling period. We find that, while TYVIX futures help improve the performance of AGG in terms of Sharpe ratios, VIX futures compare better in this dimension; at the same time, VIX futures would not help avoid the large AGG drawdowns occurred during the QE Taper Talk episode, as already noted. Importantly, overlaying AGG with VIX futures leads to a pronounced skewness, a measure of the overall sensitivity of the overlayed portfolio to drawdowns.

Table 3 reports results regarding additional ETFs and assets. Overall, TYVIX derivatives may help mitigate drawdowns on fixed income related instruments, especially when used in conjunction with VIX derivatives. Note that a systematic use of VIX derivatives might even lead to deteriorate performance in the equity space: in this space, the overlay strategy prescribes to be long VIX futures, implying, then, large insurance costs arising through contango. The last two pieces of Table 3 reveal that a systematic use of TYVIX might slightly improve overall performance, although the difference with the unhedged equity returns are both economically and statistically very negligible.

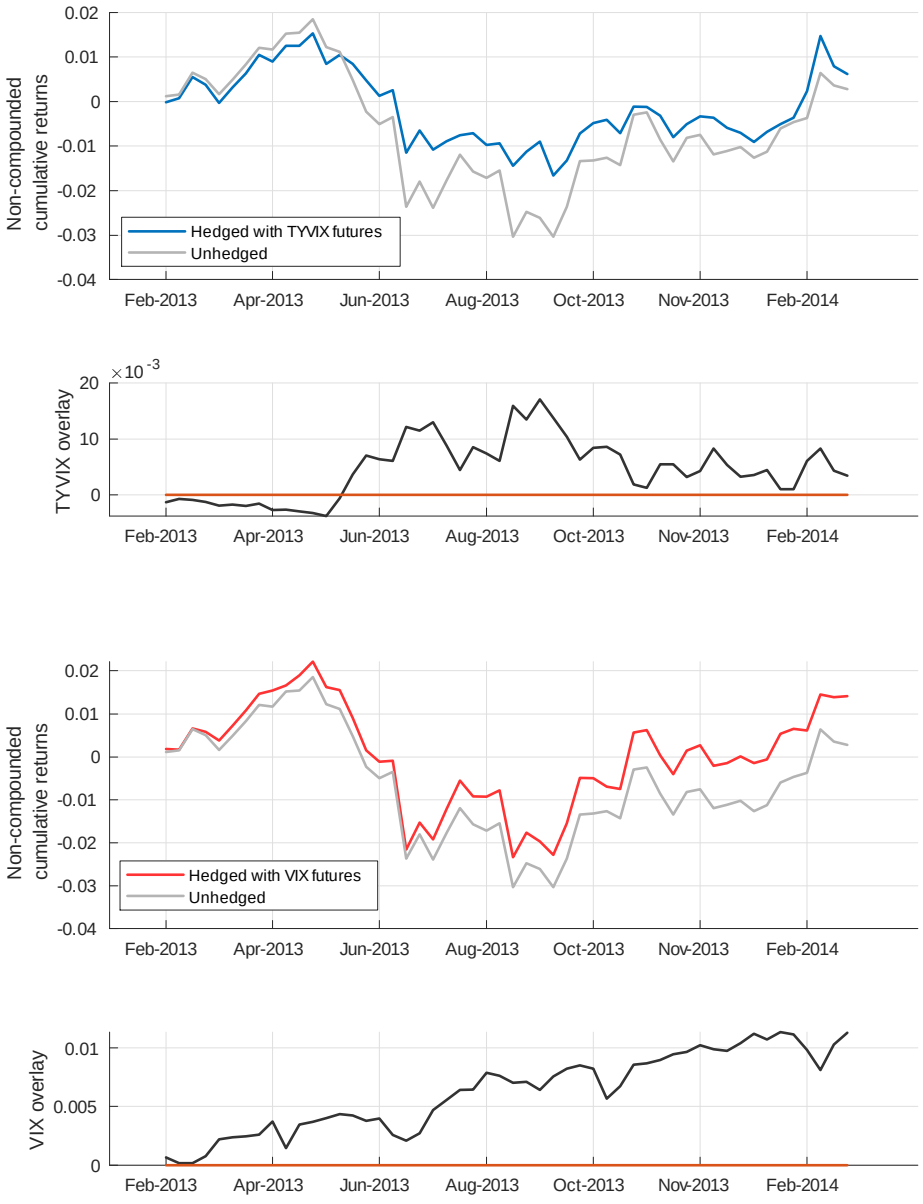

Figure 6—*Continued on the next page.*

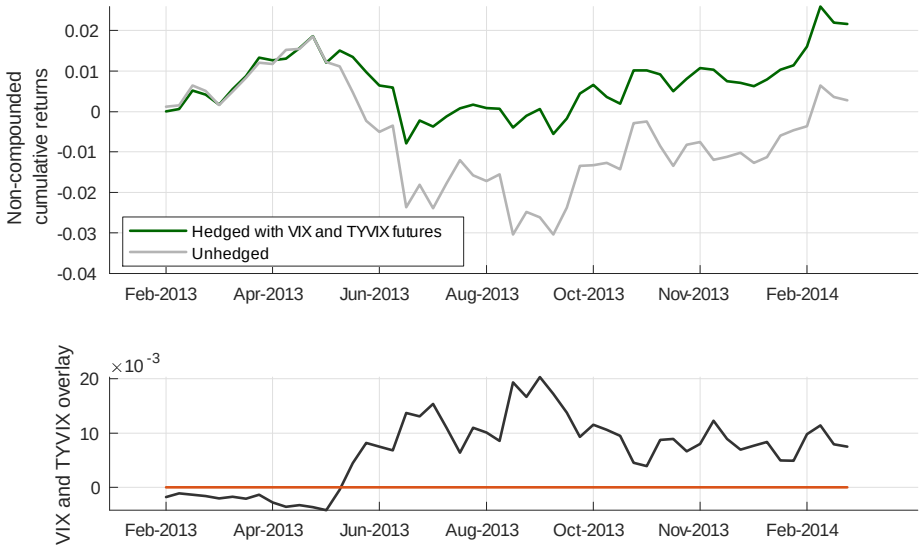

Figure 6—*Continued from the previous page.* Overlays with equity and interest rate volatility derivatives during the Taper Talk. Volatility derivatives are one-month future returns on VIX and TYVIX, and are calculated through portfolios that have an average position of 21 trading days (as in the TYVIX case depicted through the red line in Figure 4). Positioning into derivatives is determined through the coefficient of weekly rolling regressions of AGG returns onto derivative returns, with a fixed window equal to 3 years. *Top panels*: Cumulative returns from being long the iShares Core U.S. Aggregate Bond ETF, unhedged (grey line) and hedged with one month TYVIX futures (blue). *Middle panels*: Cumulative returns are as in the top panels, but hedging ratios calculated based on one month VIX futures. *Bottom panels*: Cumulative returns are as in the top panels, with hedging ratios regarding both one-month TYVIX futures and one-month VIX futures.

Table 3. Overlay performance on selected ETFs achieved through equity (vix) and interest rate (tyvix) volatility derivatives, or both (tyvix & vix). Volatility derivatives are one-month future returns on VIX and TYVIX, and are calculated through portfolios that have an average position of 21 trading days. Mean and vol columns are the average returns and standard deviations of the investment strategies, annualized; Sharpe is the Sharpe ratio defined as the ratio of annualized means to standard deviations; Skewn. is the coefficient of skewness calculated on the strategies returns; Drawdn. is the maximum drawdown on the investment strategies. Sampling period is from January 2, 2003 to February 19, 2016.

AGG.US.Equity: Treas, gvt, corp, MBS, ABS and CMBS

	mean	vol	Sharpe	Skewn.	Drawdn.
unhedged	0.0026	0.0398	0.0671	-0.9144	-0.0477
tyvix	0.0059	0.0303	0.1972	-0.4082	-0.0313
vix	0.0136	0.0405	0.3363	-0.9712	-0.0444
tyvix & vix	0.0208	0.0279	0.7464	-0.6265	-0.0260

LQD.US.Equity: Investment-grade corporate bonds

	mean	vol	Sharpe	Skewn.	Drawdn.
unhedged	0.0162	0.0729	0.2227	-1.2645	-0.0844
tyvix	0.0217	0.0559	0.3881	-0.8243	-0.0481
vix	0.0166	0.0731	0.2281	-1.2655	-0.0844
tyvix & vix	0.0308	0.0543	0.5664	-0.9050	-0.0478

TIP.US.Equity: Inflation protected T-notes

	mean	vol	Sharpe	Skewn.	Drawdn.
unhedged	-0.0609	0.0704	-0.8637	-0.9247	-0.0986
tyvix	-0.0603	0.0551	-1.0929	-0.5730	-0.0885
vix	-0.0482	0.0725	-0.6648	-0.9264	-0.0944
tyvix & vix	-0.0422	0.0547	-0.7702	-0.6413	-0.0752

TY1.Comdty: Ten Year T-note

	mean	vol	Sharpe	Skewn.	Drawdn.
unhedged	-0.0396	0.0573	-0.6925	-1.5188	-0.0797
tyvix	-0.0342	0.0473	-0.7214	-1.3031	-0.0729
vix	-0.0126	0.0588	-0.2148	-1.5298	-0.0624
tyvix & vix	-0.0026	0.0434	-0.0602	-1.6840	-0.0487

TLT.US.Equity: Treasury bonds (>20 years)

	mean	vol	Sharpe	Skewn.	Drawdn.
unhedged	-0.0503	0.1257	-0.4003	-0.3346	-0.1666
tyvix	-0.0321	0.1067	-0.3007	-0.1014	-0.1408
vix	0.0505	0.1305	0.3870	-0.3681	-0.1403
tyvix & vix	0.0797	0.0904	0.8810	-0.1783	-0.0805

SHY.US.Equity: Treasury bonds ($\in [1, 3]$ years)

	mean	vol	Sharpe	Skewn.	Drawdn.
unhedged	0.0040	0.0049	0.8151	-0.5283	-0.0031
tyvix	0.0049	0.0044	1.1254	-0.5862	-0.0021
vix	0.0060	0.0052	1.1626	-0.6315	-0.0030
tyvix & vix	0.0072	0.0045	1.5924	-0.8048	-0.0020

Table 3 continued

PZA.US.Equity: Muni bonds (>20 years)

	mean	vol	Sharpe	Skewn.	Drawdn.
unhedged	-0.0409	0.0786	-0.5210	-0.9045	-0.1187
tyvix	-0.0385	0.0742	-0.5187	-0.8962	-0.1027
vix	-0.0288	0.0795	-0.3621	-0.9568	-0.1153
tyvix & vix	-0.0214	0.0736	-0.2913	-1.0031	-0.0948

MUB.US.Equity: Investment grade muni bonds

	mean	vol	Sharpe	Skewn.	Drawdn.
unhedged	-0.0238	0.0749	-0.3173	-1.5570	-0.0846
tyvix	-0.0212	0.0641	-0.3298	-1.3012	-0.0632
vix	-0.0221	0.0751	-0.2945	-1.5702	-0.0844
tyvix & vix	-0.0137	0.0636	-0.2162	-1.3119	-0.0633

IEI.US.Equity: Treasury bonds ($\in [3, 7]$ years)

	mean	vol	Sharpe	Skewn.	Drawdn.
unhedged	-0.0010	0.0310	-0.0322	-0.8102	-0.0383
tyvix	0.0040	0.0245	0.1657	-0.3682	-0.0240
vix	0.0133	0.0321	0.4160	-0.8825	-0.0336
tyvix & vix	0.0213	0.0228	0.9332	-0.6697	-0.0167

IEF.US.Equity: Treasury bonds ($\in [7, 10]$ years)

	mean	vol	Sharpe	Skewn.	Drawdn.
unhedged	-0.0181	0.0653	-0.2768	-0.7270	-0.0875
tyvix	-0.0090	0.0505	-0.1791	-0.2550	-0.0650
vix	0.0186	0.0677	0.2741	-0.7824	-0.0755
tyvix & vix	0.0339	0.0444	0.7639	-0.5026	-0.0385

SPX.Index: S&P 500 index

	mean	vol	Sharpe	Skewn.	Drawdn.
unhedged	0.1911	0.1131	1.6891	-0.3388	-0.0545
tyvix	0.1801	0.1021	1.7630	-0.3443	-0.0501
vix	0.0327	0.0514	0.6358	-0.3224	-0.0490
tyvix & vix	0.0232	0.0563	0.4115	-0.5482	-0.0556

DIA.US.Equity: Dow Jones Industrial Average

	mean	vol	Sharpe	Skewn.	Drawdn.
unhedged	0.1640	0.1097	1.4945	-0.5932	-0.0657
tyvix	0.1539	0.1014	1.5176	-0.5753	-0.0623
vix	0.0289	0.0607	0.4766	-0.3859	-0.0553
tyvix & vix	0.0205	0.0638	0.3220	-0.4650	-0.0604

5.2.3. Scenarios

This section describes a number of hypothetical developments in the government volatility curve that follow the occurrence of shocks affecting both interest rate and interest rate volatility. A prominent instance of an event leading to such shocks is the FED decision on December 16, 2015 to raise interest rates for the first time in nearly a decade. We investigate two issues. Firstly, we examine the model predictions regarding the reaction of the TYVIX future curve to *hypothetical* interest rate volatility shocks; this type of analysis is useful for the purpose of stress-testing the model in risk-management experiments, but also for evaluating trading theses. Secondly, we examine the model predictions on the TYVIX future curve at dates of particular historical interest; our objective is to use our model and reverse-engineer from the data the magnitude of the economic shocks underlying interest rate volatility developments occurring on such dates of interest as that in December 2015.

As for the futures curve reaction to given shocks, we consider experiments in which changes in current volatility might be either transitory or permanent. For example, we study how a permanent monetary policy shift may affect market expectations, by assessing how the TYVIX futures curve reacts to a permanent higher volatility of the short-term rate. We implement the experiments while feeding the model with information available to us up to December 4, 2015, about two weeks before the FED announced an increase in the target range for the federal funds rate. In all the experiments, we assume that there is a 1% upward parallel shift in the yield curve accompanied by shocks of various nature that we will describe in a moment.[13]

The left panel of Figure 7 shows the impact of shocks to short-term basis point volatility while long-term expected volatility is kept constant and equal to the estimate of m in Table 1. We interpret this shock as being a "transitory" one. We consider 25%, 50% and finally 75% increases in short-term volatility. In these scenarios, the shorter end of the futures curve is the most affected, while the longer end reverts to the long-term mean. In times of extreme uncertainty, volatility curves have been known to flatten or even invert, and this experiment shows the model predictions are consistent with such dynamics of the term structures. The right panel shows how the model futures curve reacts when we also change m upwards by the same amount as the shock in the realized variance. This scenario may be interpreted as one of a significant change in long-term monetary policy uncertainty. The model predicts that, in this case, changes in the futures curve resemble parallel shifts with a slight counterclockwise twist.

The left panel of Figure 8 summarizes how the future curve reacts to a steepening or flattening of the volatility skew. We simulate such changes in the volatility skew by increasing or decreasing TYVIX while keeping ATM volatility constant, and calculating futures values through our calibration procedure (see Eqs. (C.4)-(C.5) in Appendix C). We consider three scenarios: a TYVIX reduction by 25%, and two increases of 25% and 50%. We interpret a steepening of the skew as a transitory shock, which corresponds to a "fear wave" hitting the markets: we interpret it to be transitory precisely

[13] We repeat the experiments while assuming that no shifts occur in the yield curve, and find that results are qualitatively the same as those reported below.

because it merely affects out-of-the money options while keeping at-the-money option markets intact. The implications are indeed qualitatively the same as those in the left panel of Figure 7. In contrast, consider the right panel of Figure 8, in which we assume that at-the-money options are also affected by a fear wave, in that ATM volatilities now increase by the same percentage amount experienced by TYVIX: we interpret this experiment as one illustrating how a permanent fear in option markets translates in terms of the TYVIX futures curve. The effects are qualitatively similar as those depicted in the right panel of Figure 7, with effects on the futures curve that increase with the futures expiry.

Our second objective is to analyze the model predictions around December 16, 2015, when the FED announced to modify its targets for the federal funds rates after almost a decade of inaction. While anecdotal evidence suggests that the outcome of this decision seemed to be largely anticipated by the market, Figure 9 shows that the TYVIX curve predicted by the model goes from contango to a sharp backwardation in a matter of a few days (from the 4th of December to just two days before the announcement). During these days, the model-implied short-term variance (v_t^2) rose by 44% whereas long-term uncertainty (μ_t) went through a 4-fold increase. Yet the model predicts a volatility market in backwardation, a situation persisting for several weeks in January 2016 (as exemplied by the TYVIX curve on January 19), a month marked by additional concerns on the weakening of data in emerging countries, oil prices and the stability of the global banking sector.

Why does the model predict backwardation during these episodes? The intuitive reason is that long-run Treasury uncertainty, μ_t, is also a mean-reverting process, and, according to our calibrated model, a low-persistent one: even large shocks on μ_t are short-lived. With shocks on μ_t absorbed relatively rapidly, the short- and medium-term future curve increases more than the long-term, producing backwardation in the volatility market during these months of heightened volatility.

To illustrate these properties throughout a simple case, consider a one-month future on the fair value of a hypothetical variance swap on the basis-point short-term rate. The fair value of this contract is

$$\mathrm{VS}_t(T) \equiv \frac{1}{T-t}\int_t^T \mathbb{E}\left(v_s^2 \middle| v_t^2, \mu_t\right) ds.$$

Assume for simplicity that $t = T - t = \Delta = \frac{1}{12}$; it can be shown that the "variance basis" at time-0 is

$$\mathsf{B}_0 \equiv F_0 - \mathrm{VS}_0(t) = \bar{\beta}\underbrace{\left(\mathbb{E}_0\left(v_t^2\right) - v_0^2\right)}_{\equiv \mathbb{E}_0(\Delta v_t^2)} + \bar{\gamma}\underbrace{\left(\mathbb{E}_0\left(\mu_t\right) - \mu_0\right)}_{\equiv \mathbb{E}_0(\Delta \mu_t)}, \tag{29}$$

where $F_0 = \mathbb{E}_0\left(\mathrm{VS}_t(T)\right)$ denotes the value of a variance future, and

$$\bar{\beta} = \frac{b_v}{\kappa_v \Delta}, \quad \bar{\gamma} = \frac{\kappa_v}{\kappa_v - \kappa_\mu}\left(\frac{b_\mu}{\kappa_\mu \Delta} - \frac{b_v}{\kappa_v \Delta}\right),$$

and $b_X = 1 - e^{-\kappa_X \Delta},\ X \in \{v, \mu\}$.

Eq. (29) tells us that, in this market, backwardation and contango are driven by mean-reversion

in the short-term (v^2) and long-term (μ^2) uncertainties. For example, the market is in contango when both current variances are "anemic" (i.e., lower then their conditionally expected values for the expiry date), and is in backwardation when they are both higher than their conditionally expected values. Now, consider a large and positive shock in both the current v_0^2 and μ_0, similarly as in the Treasury volatility market subsequent to the FED decisions in December 2015.

It is possible to show that

$$\mathbb{E}_0\left(\Delta v_t^2\right) = b_v\left(m - v_0^2\right) - \frac{\kappa_v\left(b_v - b_\mu\right)}{\kappa_v - \kappa_\mu}\left(m - \mu_0\right), \quad \mathbb{E}_0\left(\Delta \mu_t\right) = b_\mu\left(m - \mu_0\right). \tag{30}$$

The first terms of both the R.H.S. in the previous expressions capture a standard mean-reversion effect. For example, $\mathbb{E}_0\left(\Delta v_t^2\right)$ tends to be negative as v_0 gets larger. Eqs. (30) also show that a large positive shock in the long-term uncertainty (i.e., one that drives μ_0 above m) has two effects: (i) it leads $\mathbb{E}_0\left(\Delta \mu_t\right)$ to negative values, thereby being a source of backwardation (see Eq. (29)); (ii) it raises expected realized variance, $\mathbb{E}_0\left(\Delta v_t^2\right)$, thereby acting as a source of contango. Therefore, the ultimate effect of a shock in μ_0 on the variance basis B_0 is parameter dependent. In a market hit by large and positive volatility shocks (both short-term and long-term), as during December 2015 and January 2016, the effects of μ_0 are less important than those in v_0^2 when μ_t is not persistent, as in the case of our calibrated model.[14]

Naturally, the market we analyze in this paper is more complex than the variance market on the short-term rate conveyed in this example, especially due to the endogenous nature of bond price volatility. But the mechanism is similar: due to mean-reversion, our model predicts that because μ_t is a low persistent process, the TYVIX curve enters in backwardation even when long-term uncertainty, μ_t, raises more than the short-term, v_t^2.

[14] To illustrate based on the parameter values in Table 1, the two loadings on $(m - \mu_0)$ in Eqs. (30) are $-\frac{\kappa_v\left(b_v - b_\mu\right)}{\kappa_v - \kappa_\mu} = -3.5073 \cdot 10^{-2}$ and $b_\mu = 0.9644$. The former is one order of magnitude lower than the latter.

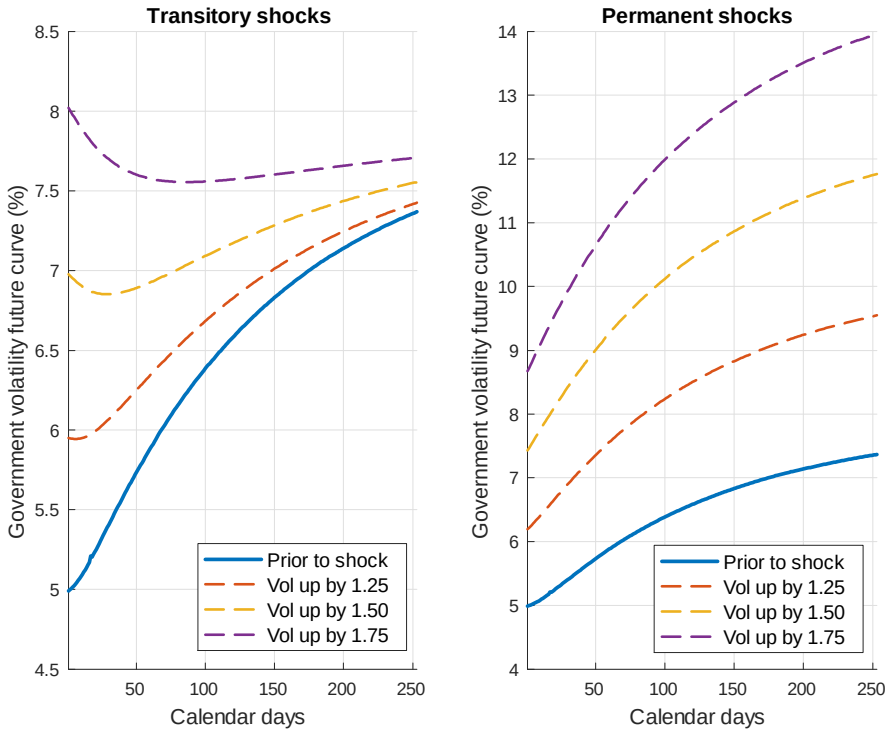

Figure 7. Changes in the TYVIX futures curve in reaction to shocks in the current short-term volatility of 25%, 50% and 75%. *Left panel*: Reaction to transitory shocks, i.e., shocks in short-term volatility that are not accompanied by changes in long-term expected volatility. *Right panel*: Reaction to permanent shocks, i.e., shocks in short-term volatility accompanied by a same magnitude changes in long-term expected volatility. In all cases, the yield curve increases parallely by 1% after the pre-shock event.

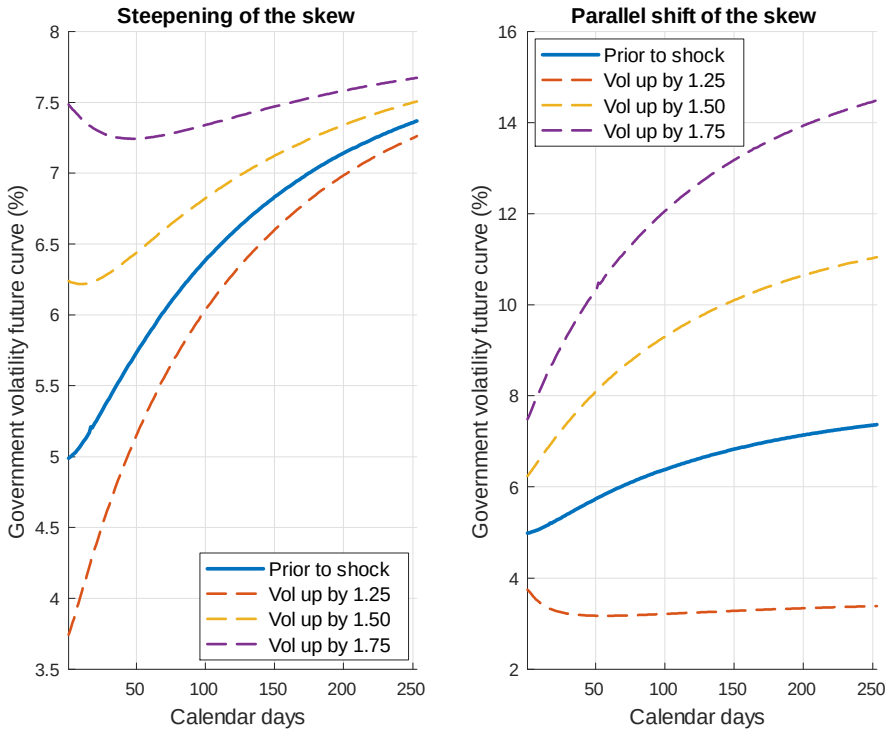

Figure 8. Changes in the TYVIX futures curve in reaction to shocks in the option skew. *Left panel*: Reaction to a steepening of the option skew, defined as an increase in TYVIX by -25%, 25% and 50% occurring while the ATM volatility remains constant. *Right panel*: Reaction to a parallel shift of the option skew, defined as an increase in TYVIX by -25%, 25% and 50% occurring while the ATM volatility changes by the same percentage amount. In all cases, the yield curve increases parallely by 1% after the pre-shock event.

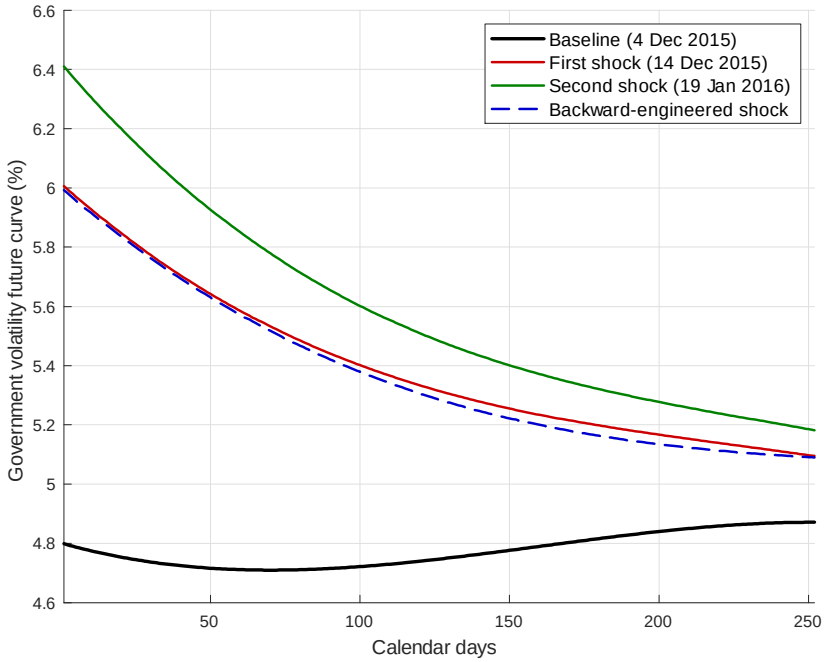

Figure 9. Model-based TYVIX futures curve on selected dates: (i) the baseline date, December 4, 2015; (ii) December 14, 2015, i.e., two days prior to the FED announcement regarding decisions on interest rates (in red, the futures curve predicted by the model with interest rate data available at that date; in blue, the futures curve predicted by the model on December 4, on the basis of the economic shocks realized in the midst of highly volatile global market conditions, i.e., from December 4 through December 14); (iii) January 19, 2016.

5.2.4. Option evaluation and the volatility of volatility

We use the calibrated model and predict hypothetical values for European-style options on TYVIX futures. Note that the option pricing model in Section 4 is referenced to options written on TYVIX, not TYVIX futures (see Eq. (24)). However, options on TYVIX futures seem to be more natural candidates than options on TYVIX as potential listed products. Their pricing is more complex, though: by standard arguments, the TYVIX future option price counterpart to the TYVIX option in Eq. (24) is

$$\begin{aligned}&\hat{\mathcal{C}}_t^f(t, v_t^2, \mu_t; t+\Delta, K, T, S, \mathbb{T}) \\ &\equiv P_t(T) \iint \left(\hat{\mathcal{F}}(\Upsilon_{T+\Delta,\mathbb{T}+\Delta}, x, y; T+\delta, T, S, \mathbb{T}) - K\right)^+ f_\Delta^F\left(x, y \middle| v_t^2, \mu_t\right) dxdy, \end{aligned} \tag{31}$$

where $\hat{\mathcal{F}}(\cdot)$ (and remaining notation) is as in Eq. (22). In particular, Eq. (31) reveals that, in addition to the double integration needed to determine $\hat{\mathcal{F}}(\cdot)$ at time $T+\delta$, one needs to integrate twice again to obtain the option value. It is computationally prohibitive, because the densities f_δ and f_Δ^F are also only known up to the solution to Riccati's equations. Appendix C.2 described an approximation to $\hat{\mathcal{C}}_t^f(t, v_t^2, \mu_t; t+\Delta, K, T, S, \mathbb{T})$, which we employ in this section (see Eq. (C.8)).

We consider options maturing in one month, with underlying futures expiring in two months. Figure 10 depicts estimates of the at-the-money Black's implied volatility on these TYVIX future option values, where the at-the-money prices are taken to be the benchmark future values (i.e., $\mathcal{F}_n^\$$ in Eq. (C.6) of Appendix C.1).

The dynamics of this *volatility of volatility* (vol-of-vol) provide useful information. Note that the vol-of-vol is a proxy for expected volatility in TYVIX corrected by risk, that is, a price for being insured against imminent (one month) volatility in TYVIX. Figure 10 contrasts this vol-of-vol with the dynamics of TYVIX. According to the model, the market evaluation of this type of insurance had anticipated the occurrence of the subprime mortgage turmoil erupting in 2007: signs of future distress could be read in the sudden increase of the vol-of-vol since 2006, an increase likely driven by a rapid succession of increases in the FED funds rate targets. Remarkably, the vol-of-vol also spikes during episodes of acute uncertainty such as the Lehman's bankruptcy, although with limited persistence. Episodes of high and persistent vol-of-vol occur during the taper tantrum of 2013: not only does TYVIX increase during this episode, the vol-of-vol fluctuates quite considerably around and prior to statements of Fed officials in May 2013. Finally the Fed increase in the target is preceded by one of the most spectacular increases in the vol-of-vol since its inception. Our model, albeit only calibrated to match expected interest rate volatility, suggests that the volatility of fixed income volatility may contain useful information on important market developments.

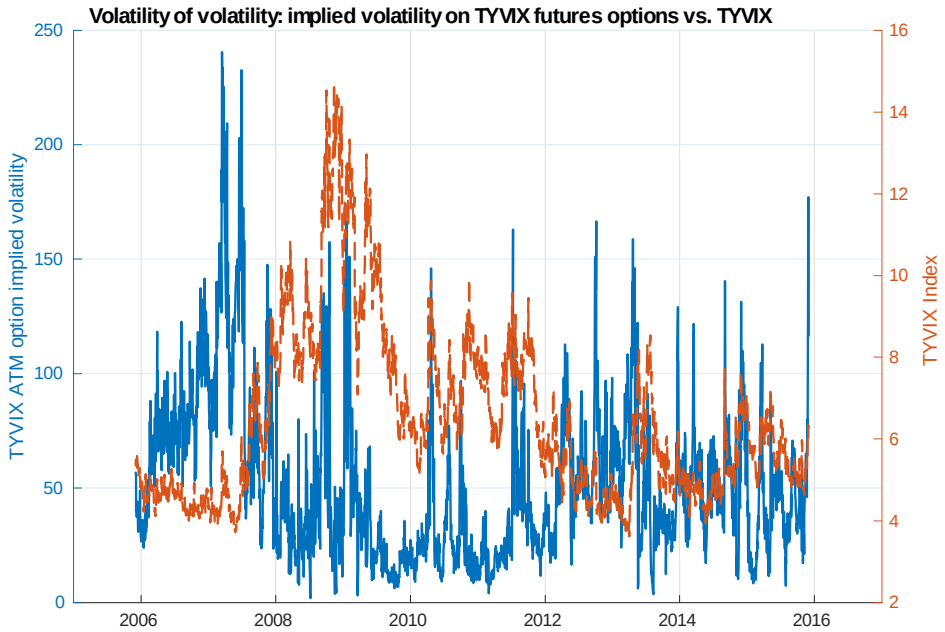

Figure 10. *Solid line*: Implied volatilities calculated on hypothetical at-the-money one-month options on TYVIX futures, with futures maturing in two months. *Dashed line*: TYVIX Index.

6. Conclusions

This paper develops a novel model of the term structure of interest rates, which we use to price government bond volatility. The model may be used for a variety of purposes, such as risk-management or hedging of fixed income portfolios, but also for extracting information on unobservable variables such as those likely to affect or reflect short-term or long-term uncertainty in monetary policy. We have illustrated the use of our model in each of these domains.

An important feature of Treasury volatility markets is to be more often in backwardation than in contango. Thus, overlays of fixed income portfolios with fixed income volatility derivatives lead to mitigate the occurrence of drawdowns while avoiding large insurance costs. Our model suggests that backwardation may be a persistent episode because long-term uncertainty is mean-reverting at a fast pace. Shocks on the government volatility curve then tend to affect the short-end of the curve more than the long-term, just as it happened at the time the Federal Reserve raised interest rates in December 2015, the first time after many years of inaction. We have achieved these conclusions while calibrating the model to derivative data on interest rate volatility, but we have used the very same calibrated model to predict the behavior of the volatility of volatility, that is, the implied volatility of hypothetical options referenced to government bond volatility futures. We provide evidence that this volatility of volatility has anticipatory power regarding market distress and, thus, may be used as a

new instrument to monitor adverse market movements. Important topics for future research include the use of our model predictions to understand how government bond volatility connects to broader macroeconomic developments.

Appendix A: Preliminary results regarding a two-factor model

Our analysis relies on the three-factor model in Sections 3 and 4, but it is useful to initially base our derivations on a simpler, two-factor model. This two-factor model helps illustrate properties of the three-factor, and does actually play an auxiliary role in our calibration strategy (see Appendix C). Consider the following dynamics of the short-term rate:

$$\left\{ \begin{array}{lcl} dr_\tau &=& \kappa_r \left(\theta_\tau - r_\tau\right) d\tau + v_\tau dW_{1\tau} \\ dv_\tau^2 &=& \kappa_v \left(\mu - v_\tau^2\right) d\tau + \xi v_\tau \left(\rho dW_{1\tau} + \sqrt{1-\rho^2} dW_{2\tau}\right) \end{array} \right. \tag{A.1}$$

These dynamics are easily seen to be special case of Eqs. (8) in the main text (notably when the long-term uncertainty factor μ_τ is constant and equal to μ). We have:

PROPOSITION A.1. *Assume that the short-term rate is as in Eqs. (A.1). Then, the price at time $\tau \geq t$ of a zero coupon bond expiring at time S, when the state is (r_τ, v_τ), is*

$$P_\tau \left(r_\tau, v_\tau^2, S\right) \equiv e^{A_S(\tau) - B_S(\tau) r_\tau + C_S(\tau) v_\tau^2}, \tag{A.2}$$

where

$$A_S(\tau) = -\int_\tau^S B_S(u) \kappa_r \theta_u du + \kappa_v \mu \int_\tau^S C_S(u) du, \quad B_S(\tau) = \frac{1 - e^{-\kappa_r (S-\tau)}}{\kappa_r}, \tag{A.3}$$

and $C_S(\tau)$ is the solution to the following Riccati's equation,

$$\dot{C}_S(\tau) = \left(\kappa_v + \rho \xi B_S(\tau)\right) C_S(\tau) - \frac{1}{2}\left(B_S^2(\tau) + \xi^2 C_S^2(\tau)\right), \quad C_S(S) = 0, \tag{A.4}$$

and the dot indicates differentiation with respect to time τ. Finally, set the parameter θ_τ to

$$\kappa_r \theta_\tau = \frac{\partial f_\$(t,\tau)}{\partial \tau} + \kappa_r \left(f_\$(t,\tau) + \frac{\partial C_\tau(t)}{\partial \tau} v_t^2 + \kappa_v \mu \int_t^\tau \frac{\partial C_\tau(u)}{\partial \tau} du\right) + \frac{\partial^2 C_\tau(t)}{\partial \tau^2} v_t^2 + \kappa_v \mu \int_t^\tau \frac{\partial^2 C_\tau(u)}{\partial \tau^2} du, \tag{A.5}$$

where $f_\$(t,\tau)$ denotes an hypothetically observed instantaneous forward rate at time t for maturity τ. Then, the price predicted by the model matches the yield curve observed at t, viz

$$P_t\left(r_t, v_t^2, S\right) = e^{-\int_t^S f_\$(t,\tau) d\tau} \equiv P_t^\$(S) \quad \textit{for all } S,$$

where $P_t^\$(S)$ denotes the market price of a zero coupon bond at t and expiring at S.

PROOF OF PROPOSITION A.1. By standard arguments, the pricing function in Eq. (A.2) holds with the three functions, $A_S(\cdot)$, $B_S(\cdot)$ and $C_S(\cdot)$ given in the proposition. To determine the infinite dimensional parameter θ_τ in Eq. (A.5), we match the instantaneous forward rate predicted by the model at t, say $f_t\left(r_t, v_t^2, S\right) \equiv -\frac{\partial \ln P_t(r_t, v_t^2, S)}{\partial S}$, to $f_\$(t,S)$, leaving

$$\begin{aligned} f_\$(t,S) &= f_t\left(r_t, v_t^2, S\right) \\ &= -\frac{\partial A_S(t)}{\partial S} + \frac{\partial B_S(t)}{\partial S} r_t - \frac{\partial C_S(t)}{\partial S} v_t^2, \\ &= \kappa_r \int_t^S e^{-\kappa_r (S-u)} \theta_u du - \kappa_v \mu \int_t^S \frac{\partial C_S(u)}{\partial S} du + e^{-\kappa_r (S-t)} r_t - \frac{\partial C_S(t)}{\partial S} v_t^2, \end{aligned} \tag{A.6}$$

where the last equality follows by differentiating the expressions for $A_S(\tau)$ and $B_S(\tau)$ in Eqs. (A.3).

Let us differentiate both sides of Eq. (A.6) with respect to S, leaving,

$$\frac{\partial f_{\$}(t,S)}{\partial S} = \kappa_r \left(\theta_S - \kappa_r \int_t^S e^{-\kappa_r (S-u)} \theta_u du \right) - \kappa_v \mu \int_t^S \frac{\partial^2 C_S(u)}{\partial S^2} du - \kappa_r e^{-\kappa_r (S-t)} r_t - \frac{\partial^2 C_S(t)}{\partial S^2} v_t^2. \quad \text{(A.7)}$$

By replacing Eq. (A.6) into the R.H.S. of Eq. (A.7), and rearranging terms, leads to Eq. (A.5).

Next, we verify θ_τ in Eq. (A.5) is indeed the infinite dimensional parameter we are searching for. Replacing Eq. (A.5) into the first term on the R.H.S. of Eq. (A.6),

$$\begin{aligned} \int_t^S e^{-\kappa_r (S-u)} \kappa_r \theta_u du = & \underbrace{\int_t^S e^{-\kappa_r (S-u)} \left(\frac{\partial f_{\$}(t,u)}{\partial u} + \kappa_r f_{\$}(t,u) \right) du}_{= f_{\$}(t,S) - e^{-\kappa_r (S-t)} f_{\$}(t,t)} \\ & + v_t^2 \int_t^S e^{-\kappa_r (S-u)} \left(\kappa_r \frac{\partial C_u(t)}{\partial u} + \frac{\partial^2 C_u(t)}{\partial u^2} \right) du \\ & + \kappa_v \mu \int_t^S e^{-\kappa_r (S-u)} \left(\kappa_r \int_t^u \frac{\partial C_u(x)}{\partial u} dx + \int_t^u \frac{\partial^2 C_u(x)}{\partial u^2} dx \right) du, \end{aligned} \quad \text{(A.8)}$$

where the equality below the first term of the R.H.S. of Eq. (A.8) follows by integrating by parts. By plugging Eq. (A.8) into Eq. (A.7), using that $f_{\$}(t,t) = r_t$, and rearranging terms,

$$\begin{aligned} f_t\left(r_t, v_t^2, S\right) = & f_{\$}(t,S) + \left(\int_t^S e^{-\kappa_r (S-u)} \left(\kappa_r \frac{\partial C_u(t)}{\partial u} + \frac{\partial^2 C_u(t)}{\partial u^2} \right) du - \frac{\partial C_S(t)}{\partial S} \right) v_t^2 \\ & + \kappa_v \mu \left(\int_t^S e^{-\kappa_r (S-u)} \left(\kappa_r \int_t^u \frac{\partial C_u(x)}{\partial u} dx + \int_t^u \frac{\partial^2 C_u(x)}{\partial u^2} dx \right) du - \int_t^S \frac{\partial C_S(x)}{\partial S} dx \right). \end{aligned} \quad \text{(A.9)}$$

We show that the second and the third terms of Eq. (A.9) are zero. As for the second term, we have that by an integration by parts,

$$\int_t^S e^{-\kappa_r (S-u)} \left(\kappa_r \frac{\partial C_u(t)}{\partial u} + \frac{\partial^2 C_u(t)}{\partial u^2} \right) du = \left[e^{-\kappa_r (S-u)} \frac{\partial C_u(t)}{\partial u} \right]_{u=t}^{u=S} = \frac{\partial C_S(t)}{\partial S}, \quad \text{(A.10)}$$

because by evaluating the Riccati's equation (A.4) in $\tau = S$ delivers $\frac{\partial C_y(y)}{\partial y} \equiv \dot{C}_S(\tau)\Big|_{\tau=S=y} = 0$ for all y. As for the third term,

$$\begin{aligned} & \int_t^S \left(\int_t^u e^{-\kappa_r (S-u)} \left(\kappa_r \frac{\partial C_u(x)}{\partial u} + \frac{\partial^2 C_u(x)}{\partial u^2} \right) dx \right) du \\ & = \int_t^S \left(\int_x^S e^{-\kappa_r (S-u)} \left(\kappa_r \frac{\partial C_u(x)}{\partial u} + \frac{\partial^2 C_u(x)}{\partial u^2} \right) du \right) dx \\ & = \int_t^S \frac{\partial C_S(x)}{\partial S} dx \end{aligned}$$

where the first equality follows by Fubini, and the second by Eq. (A.10). ■

Figure A.1 reports theoretical and observed yield curves on selected dates of our sample. Theoretical values are obtained with the parameter values in Table 1 of the main text (Section 5), and relying on Eq. (A.5) of Proposition 2.

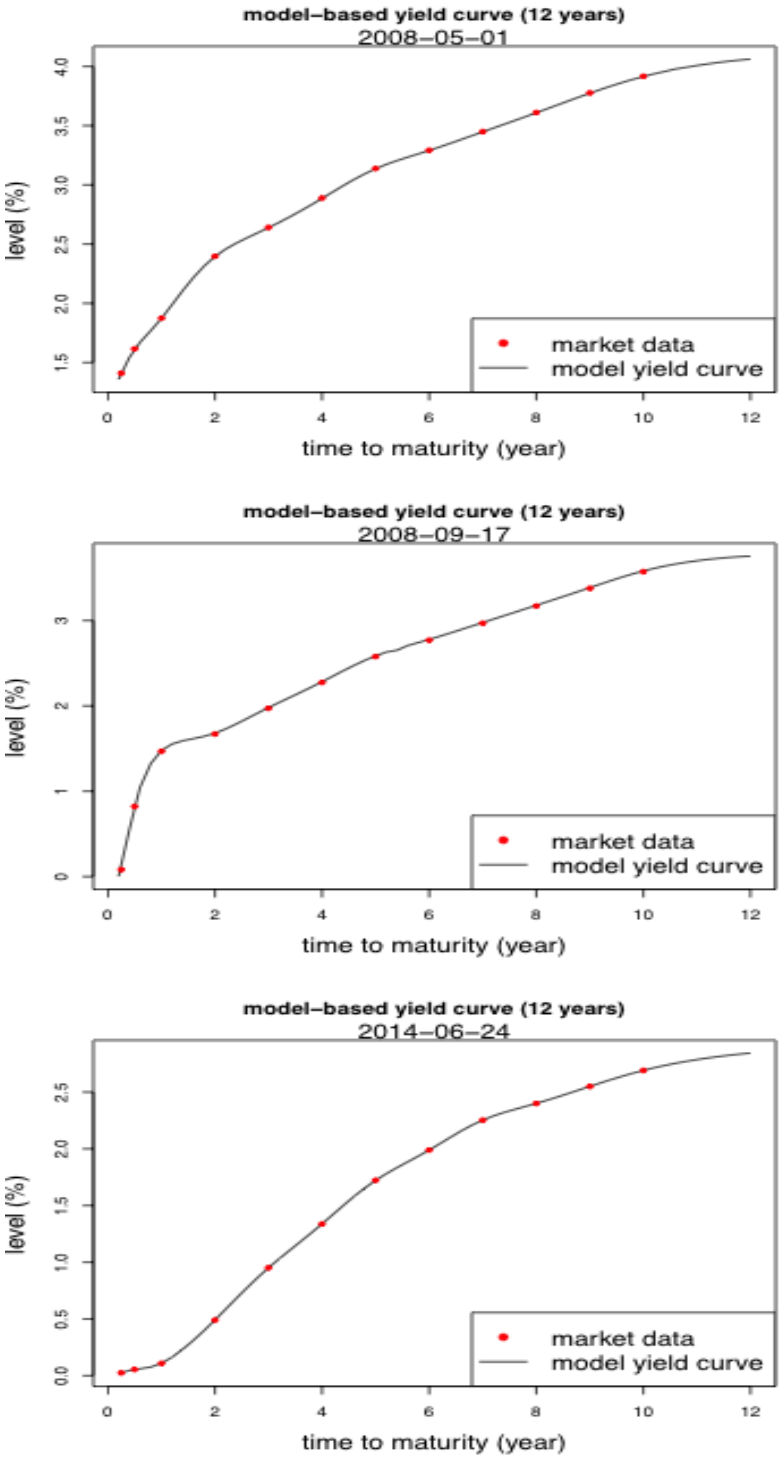

Figure A.1. Yield curves on selected days and model's reconstructions based on the calibration of the infinite dimensional parameter θ_τ through Eq. (A.5).

By design, the infinite-dimension parameter θ_τ allows an exact fit of the yield curve on any given date as illustrated by Figure A.1, ensuring internal consistency between market-observed yields and the instantaneous variance of coupon-bearing government bond returns.

Next, we derive results on the volatility predicted by the model based on Proposition A.1. By Eq. (1), the price of a forward on a coupon bearing bond is

$$F_t\left(S,\mathbb{T}\right)\equiv F_t\left(r_t,v_t^2,S,\mathbb{T}\right)\equiv\sum_{i=i_t}^{N}\frac{C_i}{n}F_t^z\left(r_t,v_t^2,S,T_i\right)+F_t^z\left(r_t,v_t^2,S,\mathbb{T}\right), \tag{A.11}$$

where

$$F_t^z\left(S,T_o\right)\equiv F_t^z\left(r_t,v_t^2,S,T_o\right)\equiv\frac{P_t\left(r_t,v_t^2,T_o\right)}{P_t\left(r_t,v_t^2,S\right)}. \tag{A.12}$$

We develop predictions regarding the volatility of this two-factor model based on Eqs. (A.11)-(A.12). First, we focus on the zero coupon bond case and determine its realized variance and a forward looking volatility index (see Eqs. (A.17) and (A.21)); and second, we deal with the coupon bearing case (see Eq. (A.26)).

Dynamics of forwards on zero coupon bonds. Below, we show that

$$\left\{\begin{array}{lcl}\dfrac{dF_\tau^z\left(S,T_o\right)}{F_\tau^z\left(S,T_o\right)} & = & v_\tau^2\Psi_\tau\left(T,S,T_o\right)d\tau+v_\tau\left(v_{1\tau}^z\left(S,T_o\right)dW_{1\tau}^T+v_{2\tau}^z\left(S,T_o\right)dW_{2\tau}^T\right)\\ dv_\tau^2 & = & \left(\kappa_v\mu-G_T\left(\tau\right)v_\tau^2\right)d\tau+\xi v_\tau\left(\rho dW_{1\tau}^T+\sqrt{1-\rho^2}dW_{2\tau}^T\right)\end{array}\right. \tag{A.13}$$

where $dW_{1\tau}^T$ and $dW_{2\tau}^T$ are two independent Brownian motions under the forward probability Q_T, $\Psi_\tau\left(T,S,T_o\right)$ is a deterministic function (see Eq. (A.23) below), and

$$v_{i\tau}^z\left(S,T_o\right)=\varphi_{i\tau}\left(T_o\right)-\varphi_{i\tau}\left(S\right),\quad i=1,2, \tag{A.14}$$

and for a generic $\mathcal{X}$,

$$\varphi_{1\tau}\left(\mathcal{X}\right)\equiv-B_{\mathcal{X}}\left(\tau\right)+\xi\rho C_{\mathcal{X}}\left(\tau\right),\quad\varphi_{2\tau}\left(\mathcal{X}\right)\equiv\xi\sqrt{1-\rho^2}C_{\mathcal{X}}\left(\tau\right), \tag{A.15}$$

and, finally, $G_T\left(\tau\right)$ is a time-varying speed of mean-reversion of basis point variance v_τ^2 under Q_T,

$$G_T\left(\tau\right)\equiv\kappa_v+\xi\left(\rho B_T\left(\tau\right)-\xi C_T\left(\tau\right)\right),\quad\tau\in\left[t,T\right]. \tag{A.16}$$

Realized and risk-adjusted expected variance on zero coupon bonds. Next, recall the definition of $v_\tau^z\left(v_\tau;S,T_o\right)$ in the main text, $v_\tau^z\left(v_\tau;S,T_o\right)=v_\tau\times\left[v_{1\tau}^z\left(S,T_o\right)\quad v_{2\tau}^z\left(S,T_o\right)\right]$. By a direct calculation,

$$\left\|v_\tau^z\left(v_\tau;S,T_o\right)\right\|^2\equiv\phi_\tau^z\left(S,T_o\right)\cdot v_\tau^2, \tag{A.17}$$

where

$$\phi_\tau^z\left(S,T_o\right)\equiv\left(B_{T_o}\left(\tau\right)-B_S\left(\tau\right)\right)^2+\xi^2\left(C_{T_o}\left(\tau\right)-C_S\left(\tau\right)\right)^2-2\rho\xi\left(B_{T_o}\left(\tau\right)-B_S\left(\tau\right)\right)\left(C_{T_o}\left(\tau\right)-C_S\left(\tau\right)\right), \tag{A.18}$$

which follows by calculating the instantaneous variance of the forward price in Eq. (A.13).

Next, by taking expectations of the basis point variance process v_τ^2 in the second of Eqs. (A.13), we obtain that for all τ,

$$\mathbb{E}_t^{Q_T}\left(v_\tau^2\right)=\kappa_v\mu\int_t^\tau e^{-\int_s^\tau G_T\left(u\right)du}ds+e^{-\int_t^\tau G_T\left(u\right)du}\cdot v_t^2.$$

Replacing the previous expectation into the expectation of the annualized integrated variance under Q_T leaves,

$$\frac{1}{T-t}\int_t^T \mathbb{E}_t^{Q_T}\left(\left\|v_\tau^z\left(v_\tau;S,T_o\right)\right\|^2\right)d\tau=\kappa_v\mu\mathcal{A}_1^z\left(t,T,S,T_o\right)+\mathcal{A}_2^z\left(t,T,S,T_o\right)\cdot v_t^2, \tag{A.19}$$

where we have used Eq. (A.17) to evaluate $\left\|v_\tau^z\left(v_\tau;S,T_o\right)\right\|^2$, and

$$\begin{aligned}\mathcal{A}_1^z\left(t,T,S,T_o\right)\equiv&\ \frac{1}{T-t}\int_t^T\left(\int_t^\tau e^{-\int_s^\tau G_T(u)\,du}ds\right)\phi_\tau^z\left(S,T_o\right)d\tau,\\ \mathcal{A}_2^z\left(t,T,S,T_o\right)\equiv&\ \frac{1}{T-t}\int_t^T e^{-\int_t^\tau G_T(u)\,du}\phi_\tau^z\left(S,T_o\right)d\tau.\end{aligned} \tag{A.20}$$

Therefore, in this two-factor model, the index of percentage volatility in Eq. (7) predicted by Proposition 3 specializes to

$$\text{GB-VI}^z\left(v_t^2;t,T,S,T_o\right)\equiv\sqrt{\kappa_v\mu\mathcal{A}_1^z\left(t,T,S,T_o\right)+\mathcal{A}_2^z\left(t,T,S,T_o\right)\cdot v_t^2},\quad t\leq T\leq S\leq T_o, \tag{A.21}$$

where $\phi_\tau^z\left(S,T_o\right)$ and $A_j^z\left(t,T,S,T_o\right)$ are the two constants given in Eqs. (A.18) and (A.20).

Proof of Eqs. (A.13). By Eq. (A.2), and Itô's lemma, the price of a zero coupon bond expiring at any fixed $\mathcal{X}$, $P_\tau\left(\mathcal{X}\right)\equiv P_\tau\left(r_\tau,v_\tau,\mathcal{X}\right)$, satisfies

$$\frac{dP_\tau\left(\mathcal{X}\right)}{P_\tau\left(\mathcal{X}\right)}=r_\tau d\tau+v_\tau\left(\varphi_{1\tau}\left(\mathcal{X}\right)dW_{1\tau}+\varphi_{2\tau}\left(\mathcal{X}\right)dW_{2\tau}\right),$$

where $\varphi_{1\tau}\left(\mathcal{X}\right)$ and $\varphi_{2\tau}\left(\mathcal{X}\right)$. By a standard argument, we can define two standard Brownian motions under the forward probability Q_T, $dW_{i\tau}^T=dW_{i\tau}-v_\tau\varphi_{i\tau}\left(T\right)d\tau$, $i=1,2$, such that by Girsanov theorem, one has that under Q_T,

$$\frac{dP_\tau\left(\mathcal{X}\right)}{P_\tau\left(\mathcal{X}\right)}=\left(r_\tau+v_\tau^2\left(\varphi_{1\tau}\left(\mathcal{X}\right)\varphi_{1\tau}\left(T\right)+\varphi_{2\tau}\left(\mathcal{X}\right)\varphi_{2\tau}\left(T\right)\right)\right)d\tau+v_\tau\left(\varphi_{1\tau}\left(\mathcal{X}\right)dW_{1\tau}^T+\varphi_{2\tau}\left(\mathcal{X}\right)dW_{2\tau}^T\right), \tag{A.22}$$

where the two functions, $\varphi_{i\tau}$, are as in Eqs. (A.15). Applying Itô's lemma to the forward price predicted by the model,

$$F_t^z\left(S,T_o\right)=\frac{P_t(r_t,v_t^2,\mathcal{X})\big|_{\mathcal{X}=T_o}}{P_t(r_t,v_t^2,\mathcal{X})|_{\mathcal{X}=S}},$$

and utilizing Eq. (A.22), yields the first of Eqs. (A.13), with

$$\Psi_\tau\left(T,S,T_o\right)\equiv\sum_{i=1}^2 v_{i\tau}^z\left(S,T_o\right)v_{i\tau}^z\left(S,T\right). \tag{A.23}$$

Finally, the second of Eqs. (A.13) follows by a change of probability in Eq. (A.1), leading to the time-varying speed of mean-reversion in Eq. (A.16). ■

Government bond volatility index. Next, we determine the government bond index based on the two-factor model. By Eqs. (17) and (A.13), the instantaneous variance of the forward returns is

$$\left\|v_\tau\left(v_\tau;S,\mathbb{T}\right)\right\|^2\equiv\left(\left(\sum_{j=i_t}^N\omega_\tau^j\left(S,\mathbb{T}\right)v_{1\tau}^z\left(S,T_j\right)\right)^2+\left(\sum_{j=i_t}^N\omega_\tau^j\left(S,\mathbb{T}\right)v_{2\tau}^z\left(S,T_j\right)\right)^2\right)\cdot v_\tau^2, \tag{A.24}$$

where the functions $v^{z}_{i\tau}\left(S,T_j\right)$ are defined as in Eq. (A.14). Set $\omega^j_\tau\left(S,\mathbb{T}\right)\approx\omega^j_t\left(S,\mathbb{T}\right)$ in Eq. (A.24), or,

$$\left\|v_\tau\left(v_\tau;S,\mathbb{T}\right)\right\|^2\approx\alpha_\tau(\mathsf{Y}^{\$}_{t,\mathbb{T}},S,\mathbb{T})\cdot v^2_\tau, \tag{A.25}$$

where

$$\alpha_\tau(\mathsf{Y}^{\$}_{t,\mathbb{T}},S,\mathbb{T})\equiv\left(\sum_{j=i_t}^{N}\omega^j_t\left(S,\mathbb{T}\right)v^{z}_{1\tau}\left(S,T_j\right)\right)^2+\left(\sum_{j=i_t}^{N}\omega^j_t\left(S,\mathbb{T}\right)v^{z}_{2\tau}\left(S,T_j\right)\right)^2,$$

and the dependence on $\mathsf{Y}^{\$}_{t,\mathbb{T}}$ arises through the weights $\omega^j_t\left(S,\mathbb{T}\right)$ in Eq. (17).

Based on (A.25), we can now determine the government bond volatility index by calculations similar to those leading to Eq. (A.19):

$$\text{GB-VI}(\mathsf{Y}^{\$}_{t,\mathbb{T}},v^2_t;t,T,S,\mathbb{T})=\sqrt{\kappa_v\mu\mathcal{A}_1(\mathsf{Y}^{\$}_{t,\mathbb{T}},T,S,\mathbb{T})+\mathcal{A}_2(\mathsf{Y}^{\$}_{t,\mathbb{T}},T,S,\mathbb{T})v^2_t}, \tag{A.26}$$

where

$$\begin{aligned}\mathcal{A}_1(\mathsf{Y}^{\$}_{t,\mathbb{T}},T,S,\mathbb{T})=&\quad\frac{1}{T-t}\int_t^T\left(\int_t^\tau e^{-\int_s^\tau G_T\left(u\right)du}ds\right)\alpha_\tau(\mathsf{Y}^{\$}_{t,\mathbb{T}},S,\mathbb{T})d\tau,\\ \mathcal{A}_2(\mathsf{Y}^{\$}_{t,\mathbb{T}},T,S,\mathbb{T})=&\quad\frac{1}{T-t}\int_t^T e^{-\int_t^\tau G_T\left(u\right)du}\alpha_\tau(\mathsf{Y}^{\$}_{t,\mathbb{T}},S,\mathbb{T})d\tau.\end{aligned}$$

Evaluation of derivatives. Similarly as in the three-factor model in the main text, we approximate the value at t of a TYVIX future maturing at $t+\delta$ by freezing $\omega^j_{t+\delta}\left(S+\delta,\mathbb{T}+\delta\right)$ at $\omega^j_t\left(S,\mathbb{T}\right)$, obtaining

$$\hat{\mathcal{F}}(\mathsf{Y}^{\$}_{t,\mathbb{T}},v^2_t;t+\delta,T,S,\mathbb{T})\equiv\int_0^\infty\sqrt{\kappa_v\mu\mathcal{A}_1(\mathsf{Y}^{\$}_{t,\mathbb{T}},T,S,\mathbb{T})+\mathcal{A}_2(\mathsf{Y}^{\$}_{t,\mathbb{T}},T,S,\mathbb{T})x}\cdot\bar{f}_\delta\left(x\middle|\,v^2_t\right)dx, \tag{A.27}$$

where $\bar{f}_\delta\left(v^2_{t+\delta}\middle|\,v^2_t\right)$ is the transition density of $v^2_{t+\delta}$ given v^2_t under Q. It is well-known by Eqs. (A.1), this transition density is a non-central chi-square with $2\left(q+1\right)$ degrees of freedom and non-centrality parameter $2u_1$, viz

$$\bar{f}_\delta\left(v^2_{t+\delta}\middle|\,v^2_t\right)=ce^{-u_1-u_2}\left(\frac{u_2}{u_1}\right)^{q/2}I_q\left(2\sqrt{u_1u_2}\right),$$

where

$$c\equiv\frac{2\kappa_v}{\xi^2\left(1-e^{-\kappa_v\delta}\right)},\quad u_1\equiv ce^{-\kappa_v\delta}v^2_t,\quad u_2\equiv cv^2_{t+\delta},\quad q\equiv\frac{2\kappa_v\mu}{\xi^2}-1,$$

and $I_q\left(\cdot\right)$ is the modified Bessel function of the first kind of order q.

Next, we approximate the value at t of a TYVIX European call option maturing at $t+\Delta$ and struck at K, by freezing $\omega^j_{t+\delta}\left(S+\delta,\mathbb{T}+\delta\right)$ at $\omega^j_t\left(S,\mathbb{T}\right)$, obtaining

$$\begin{aligned}&\hat{\mathcal{C}}(\mathsf{Y}^{\$}_{t,\mathbb{T}},v^2_t;t+\Delta,K,T,S,\mathbb{T})\\ &\equiv P_t\left(T\right)\int_0^\infty\left(\sqrt{\kappa_v\mu\mathcal{A}_1(\mathsf{Y}^{\$}_{t,\mathbb{T}},T,S,\mathbb{T})+\mathcal{A}_2(\mathsf{Y}^{\$}_{t,\mathbb{T}},T,S,\mathbb{T})x}-K\right)^+\cdot\bar{f}^F_\Delta\left(x\middle|\,v^2_t\right)dx,\end{aligned} \tag{A.28}$$

where $\bar{f}^F_\Delta\left(v^2_{t+\Delta}\middle|\,v^2_t\right)$ denotes the transition density of the basis point variance under the forward probability $Q_{t+\Delta}$, determined as follows. Consider, first, the conditional characteristic function of $v^2_{t+\Delta}$ given v^2_t under the forward probability $Q_{t+\Delta}$, viz

$$c^F_\Delta\left(t,v^2_t;\vartheta\right)=\mathbb{E}^{Q_{t+\Delta}}_t\left(e^{\mathrm{i}\vartheta v^2_{t+\Delta}}\right)=e^{\chi_1(t,\Delta,\vartheta)+\chi_2(t,\Delta,\vartheta)v^2_t}, \tag{A.29}$$

for two functions $\chi_1(t,\Delta,\vartheta)$ and $\chi_2(t,\Delta,\vartheta)$ to be determined below (see Eqs. (A.30)-(A.31)).

Note that by Eq. (A.13), and under $Q_{t+\Delta}$, the basis point variance v_τ^2 is solution to

$$dv_\tau^2 = \left(\kappa_v\mu - G_{t+\Delta}(\tau)\, v_\tau^2\right) d\tau + \xi v_\tau \left(\rho dW_{1\tau}^{t+\Delta} + \sqrt{1-\rho^2}dW_{2\tau}^{t+\Delta}\right), \quad \tau \in [t, t+\Delta],$$

where $G_{t+\Delta}(\tau)$ is the time-varying persistence parameter defined in Eq. (A.16). By standard arguments, we find that the two functions $\chi_1(t,\Delta,\vartheta)$ and $\chi_2(t,\Delta,\vartheta)$ in Eq. (A.29) satisfy, for $\tau \in [t, t+\Delta)$,

$$\begin{cases} 0 = \dot{\chi}_1(\tau,\Delta,\vartheta) + \kappa_v\mu\chi_2(\tau,\Delta,\vartheta) \\ 0 = \dot{\chi}_2(\tau,\Delta,\vartheta) - G_{t+\Delta}(\tau)\,\chi_2(\tau,\Delta,\vartheta) + \frac{1}{2}\xi^2\chi_2^2(\tau,\Delta,\vartheta) \end{cases} \tag{A.30}$$

with boundary conditions

$$\chi_1(t+\Delta,\Delta,\vartheta) = 0 \quad \text{and} \quad \chi_2(t+\Delta,\Delta,\vartheta) = \mathtt{i}\vartheta. \tag{A.31}$$

The transition density $\bar{f}_\Delta^F\left(v_{t+\Delta}^2 \middle| v_t^2\right)$ is the Fourier's inverse transform of $c_\Delta^F\left(t, v_t^2; \vartheta\right)$ in Eq. (A.29):

$$\bar{f}_\Delta^F\left(v_{t+\Delta}^2 \middle| v_t^2\right) = \frac{1}{2\pi}\int_{-\infty}^{\infty} e^{-\mathtt{i}\vartheta v_{t+\Delta}^2} c_\Delta^F\left(t, v_t^2; \vartheta\right) d\vartheta. \tag{A.32}$$

Appendix B: Analysis of the three-factor model

This appendix extends results in Appendix A and provides analytical details regarding the three-factor model of the main text.

Proof of Proposition 2. Follows by generalizing the arguments made to prove Proposition A.1. In particular, the functions $A_S(\cdot)$, $B_S(\cdot)$ and $A_S(\cdot)$ in the pricing function of Proposition 2 (see Eq. (9)) are

$$A_S(\tau) = -\int_\tau^S B_S(u)\,\kappa_r\theta_u du + \kappa_\mu m\int_\tau^S D_S(u)\, du, \quad B_S(\tau) = \frac{1-e^{-\kappa_r(S-\tau)}}{\kappa_r}, \tag{B.1}$$

where $C_S(\tau)$ and $C_D(\tau)$ are solutions to the following Riccati's equations

$$\dot{C}_S(\tau) = \left(\kappa_v + \rho\xi B_S(\tau)\right) C_S(\tau) - \frac{1}{2}\left(B_S^2(\tau) + \xi^2 C_S^2(\tau)\right), \quad C_S(S) = 0, \tag{B.2}$$

and

$$\dot{D}_S(\tau) = \kappa_\mu D_S(\tau) - \left(\kappa_v C_S(\tau) + \frac{1}{2}\gamma^2 D_S^2(\tau)\right), \quad D_S(S) = 0, \tag{B.3}$$

and the dot indicates differentiation with respect to time τ. Moreover, set the parameter θ_τ equal to

$$\begin{aligned} \kappa_r\theta_\tau = {} & \frac{\partial f_\$(t,\tau)}{\partial\tau} + \kappa_r\left(f_\$(t,\tau) + \frac{\partial C_\tau(t)}{\partial\tau}v_t^2 + \frac{\partial D_\tau(t)}{\partial\tau}\mu_t + \kappa_\mu m\int_t^\tau \frac{\partial D_\tau(u)}{\partial\tau}du\right) \\ & + \frac{\partial^2 C_\tau(t)}{\partial\tau^2}v_t^2 + \frac{\partial^2 D_\tau(t)}{\partial\tau^2}\mu_t + \kappa_\mu m\int_t^\tau \frac{\partial^2 D_\tau(u)}{\partial\tau^2}du, \end{aligned} \tag{B.4}$$

where $f_\$(t,\tau)$ denotes an hypothetically observed instantaneous forward rate at time t for maturity τ. Then, the price predicted by the model matches the yield curve observed at t, viz

$$P_t\left(r_t, v_t^2, \mu_t, S\right) = e^{-\int_t^S f_\$(t,\tau)\,d\tau} \equiv P_t^\$(S) \quad \text{for all } S, \tag{B.5}$$

where $P_t^{\$}(S)$ denotes the market price of a zero coupon bond at t and expiring at S.

Note that the functions B_S and C_S in (B.1) and (B.2) are the same as B_S and C_S in the two-factor model (see (A.3) and (A.4)). Moreover, if μ_τ is constant (i.e. $\kappa_\mu = \gamma = 0$) and equal to $\mu \equiv m$, the function D_S in Eq. (B.3) is solution to $\dot{D}_S(\tau) = -\kappa_v C_S(\tau)$, such that $A_S(\tau) + D_S(\tau)\mu$ in (9) collapses to $A_S(\tau)$ in (A.2). Likewise, the infinite dimensional parameter θ_τ in Eq. (B.4) collapses to that in the two-factor model in Eq. (A.5) under the same conditions ■

Proof of Eqs. (12) and Proposition 3. First, we generalize Eq. (A.22) in Appendix A and determine the dynamics of a zero coupon bond price $P_\tau(\mathcal{X}) \equiv P_\tau(r_\tau, v_\tau, \mu_\tau, \mathcal{X})$. Second, we apply Itô's lemma to $F_\tau^z(S, T_o)$ in Eq. (11) and obtain Eqs. (12) relying on the thusly determined dynamics of $P_\tau(\mathcal{X})$. We find that the drift of $\frac{dF_\tau^z}{F_\tau^z}$ in Eq. (12) is

$$m_\tau^F d\tau \equiv m_\tau^F(S, T_o)\, d\tau = \mathbb{E}_\tau^{Q_T}\left(\frac{dF_\tau^z(S, T_o)}{F_\tau^z(S, T_o)}\right) = \left(v_\tau^2 \Psi_{A\tau}(T, S, T_o) + \mu_\tau \Psi_{B\tau}(T, S, T_o)\right) d\tau, \tag{B.6}$$

where

$$\Psi_{A\tau}(T, S, T_o) = \Psi_\tau(T, S, T_o), \quad \Psi_{B\tau}(T, S, T_o) = v_{3\tau}^z(S, T_o)\, v_{3\tau}^z(S, T),$$

and $\Psi_\tau(T, S, T_o)$ is as in Eq. (A.23). The Brownian motions under Q_T are defined as $dW_{i\tau}^T = dW_{i\tau} - v_\tau \varphi_{i\tau}(T)\, d\tau$, $i = 1, 2$, and $dW_{3\tau}^T = dW_{3\tau} - \sqrt{\mu_\tau}\varphi_{3\tau}(T)\, d\tau$. Note that the two exposures in (13), $v_{1\tau}^z(S, T_o)$ and $v_{2\tau}^z(S, T_o)$, are the same as those in the two-factor version of the model (see Eqs. (A.14)), and that the function G_T in (14) is the same as in Eq. (A.16)).

The expression for the realized variance in Eq. (15) in Proposition 3 follows by a direct calculation, and the two functions $\phi_{i\tau}^z(S, T_o)$ are given by

$$\phi_{1\tau}^z(S, T_o) = \phi_\tau^z(S, T_o), \quad \phi_{2\tau}^z(S, T_o) \equiv \gamma^2 \left(D_{T_o}(\tau) - D_S(\tau)\right)^2, \tag{B.7}$$

where $\phi_\tau^z(S, T_o)$ is as in Eq. (A.18).

Finally, we derive Eq. (16) in Proposition 3. Note that by Eq. (15), the expectation of the annualized integrated government bond variance under Q_T is

$$\begin{aligned} &\frac{1}{T-t}\int_t^T \mathbb{E}_t^{Q_T}\left(\left\|v_\tau^z(v_\tau, \mu_\tau; S, T_o)\right\|^2 d\tau\right) \\ &= \frac{1}{T-t}\int_t^T \left(\phi_{1\tau}^z(S, T_o) \cdot \mathbb{E}_t^{Q_T}\left(v_\tau^2\right) + \phi_{2\tau}^z(S, T_o) \cdot \mathbb{E}_t^{Q_T}(\mu_\tau)\right) d\tau. \end{aligned} \tag{B.8}$$

The expectations under Q_T of the basis point variance v_τ^2 and long-term uncertainty μ_τ in (12) are, for all τ,

$$\begin{cases} \mathbb{E}_t^{Q_T}\left(v_\tau^2\right) = \kappa_v \int_t^\tau e^{-\int_s^\tau G_T(u)\, du} \mathbb{E}_t^{Q_T}(\mu_s)\, ds + e^{-\int_t^\tau G_T(u)\, du} \cdot v_t^2 \\ \mathbb{E}_t^{Q_T}(\mu_\tau) = \kappa_m m \int_t^\tau e^{-\int_\ell^\tau H_T(u)\, du} d\ell + e^{-\int_t^\tau H_T(u)\, du} \cdot \mu_t \end{cases}$$

Replacing the previous expectations into Eq. (B.8), and rearranging, yields Eq. (16), where the functions

$\mathcal{B}_j^z\left(t,T,S,T_o\right)$ are given by

$$\begin{aligned}
\mathcal{B}_1^z\left(t,T,S,T_o\right) &\equiv \frac{1}{T-t}\int_t^T\left(\kappa_v b_{1\tau}\left(t,T\right)\phi_{1\tau}^z\left(S,T_o\right)+b_{2\tau}\left(t,T\right)\phi_{2\tau}^z\left(S,T_o\right)\right)d\tau,\\
\mathcal{B}_2^z\left(t,T,S,T_o\right) &\equiv \frac{1}{T-t}\int_t^T e^{-\int_t^\tau G_T\left(u\right)du}\phi_{1\tau}^z\left(S,T_o\right)d\tau,\\
\mathcal{B}_3^z\left(t,T,S,T_o\right) &\equiv \frac{1}{T-t}\int_t^T\left(\kappa_v b_{3\tau}\left(t,T\right)\phi_{1\tau}^z\left(S,T_o\right)+e^{-\int_t^\tau H_T\left(u\right)du}\phi_{2\tau}^z\left(S,T_o\right)\right)d\tau,
\end{aligned}\tag{B.9}$$

and

$$\begin{aligned}
b_{1\tau}\left(t,T\right) &\equiv \int_t^\tau e^{-\int_s^\tau G_T\left(u\right)du}\left(\int_t^s e^{-\int_\ell^s H_T\left(u\right)du}d\ell\right)ds\\
b_{2\tau}\left(t,T\right) &\equiv \int_t^\tau e^{-\int_\ell^\tau H_T\left(u\right)du}d\ell,\\
b_{3\tau}\left(t,T\right) &\equiv \int_t^\tau e^{-\int_s^\tau G_T\left(u\right)du}e^{-\int_t^s H_T\left(u\right)du}ds,
\end{aligned}\tag{B.10}$$

and the two functions G_T and H_T are as in Eqs. (14). ■

Coupon bearing bonds: The integrated drift $\bar{z}\left(t,T,S,\mathbb{T}\right)$ predicted by the model. By setting $T_i\equiv T_o$ and plugging the first of Eqs. (12) into Eq. (17) leaves

$$\begin{aligned}
\frac{dF_\tau\left(S,\mathbb{T}\right)}{F_\tau\left(S,\mathbb{T}\right)} &= \sum_{i=i_t}^N\omega_\tau^i\left(S,\mathbb{T}\right)m_\tau^F\left(S,T_i\right)d\tau\\
&\quad+\sum_{i=i_t}^N\omega_\tau^i\left(S,\mathbb{T}\right)\left(v_\tau\left(v_{1\tau}^z\left(S,T_i\right)dW_{1\tau}^T+v_{2\tau}^z\left(S,T_i\right)dW_{2\tau}^T\right)+\sqrt{\mu_\tau}v_{3\tau}^z\left(S,T_i\right)dW_{3\tau}^T\right),
\end{aligned}$$

where $m_\tau^F\left(S,\cdot\right)$ is defined as in Eq. (B.6),

$$m_\tau^F\left(S,T_i\right)=v_\tau^2\Psi_{A\tau}\left(T,S,T_i\right)+\mu_\tau\Psi_{B\tau}\left(T,S,T_i\right),$$

such that by the definition of $\bar{z}$ in Proposition 1, the integrated drift predicted by the model is

$$\bar{z}\left(t,T,S,\mathbb{T}\right)=\int_t^T\sum_{i=i_t}^N\omega_\tau^i\left(S,\mathbb{T}\right)m_\tau^F\left(S,T_i\right)d\tau.\ \blacksquare\tag{B.11}$$

Proof of Proposition 4. Eq. (19) follows by setting $\omega_\tau^j\left(S,\mathbb{T}\right)\approx\omega_t^j\left(S,\mathbb{T}\right)$ in Eq. (18), such that

$$\left\|v_\tau\left(v_\tau,\mu_\tau;S,\mathbb{T}\right)\right\|^2\approx\alpha_{1\tau}(\mathsf{Y}_{t,\mathbb{T}}^{\$},S,\mathbb{T})v_\tau^2+\alpha_{2\tau}(\mathsf{Y}_{t,\mathbb{T}}^{\$},S,\mathbb{T})\mu_\tau,$$

where

$$\begin{aligned}
\alpha_{1\tau}(\mathsf{Y}_{t,\mathbb{T}}^{\$},S,\mathbb{T}) &\equiv \left(\sum_{j=i_t}^N\omega_t^j\left(S,\mathbb{T}\right)v_{1\tau}^z\left(S,T_j\right)\right)^2+\left(\sum_{j=i_t}^N\omega_t^j\left(S,\mathbb{T}\right)v_{2\tau}^z\left(S,T_j\right)\right)^2,\\
\alpha_{2\tau}(\mathsf{Y}_{t,\mathbb{T}}^{\$},S,\mathbb{T}) &\equiv \left(\sum_{j=i_t}^N\omega_t^j\left(S,\mathbb{T}\right)v_{3\tau}^z\left(S,T_j\right)\right)^2.
\end{aligned}$$

The expressions for the three functions in Eq. (19) follow by the same arguments made to derive (B.9). They

are

$$\begin{aligned}
\mathcal{B}_1(\mathsf{Y}^{\$}_{t,\mathbb{T}},T,S,\mathbb{T}) \equiv\ & \frac{1}{T-t}\int_t^T \left(\kappa_v b_{1\tau}\left(t,T\right)\alpha_{1\tau}(\mathsf{Y}^{\$}_{t,\mathbb{T}},S,\mathbb{T})+b_{2\tau}\left(t,T\right)\alpha_{2\tau}(\mathsf{Y}^{\$}_{t,\mathbb{T}},S,\mathbb{T})\right)d\tau \\
\mathcal{B}_2(\mathsf{Y}^{\$}_{t,\mathbb{T}},T,S,\mathbb{T}) \equiv\ & \frac{1}{T-t}\int_t^T e^{-\int_t^\tau G_T\left(u\right)du}\alpha_{1\tau}(\mathsf{Y}^{\$}_{t,\mathbb{T}},S,\mathbb{T})d\tau, \\
\mathcal{B}_3(\mathsf{Y}^{\$}_{t,\mathbb{T}},T,S,\mathbb{T}) \equiv\ & \frac{1}{T-t}\int_t^T \left(\kappa_v b_{3\tau}\left(t,T\right)\alpha_{1\tau}(\mathsf{Y}^{\$}_{t,\mathbb{T}},S,\mathbb{T})+e^{-\int_t^\tau H_T\left(u\right)du}\alpha_{2\tau}(\mathsf{Y}^{\$}_{t,\mathbb{T}},S,\mathbb{T})\right)d\tau
\end{aligned} \tag{B.12}$$

where the three function $b_{jt}\left(t,T\right)$ are as in Eqs. (B.10) and the two functions G_T and H_T are as in Eqs. (14).

Derivation of the transition densities in (22) and (24). We first determine $f_\delta\left(x,y|\,v_t^2,\mu_t\right)$ in (22)—the transition density $\left(v_{t+\Delta}^2,\mu_{t+\Delta}\right)$ given $\left(v_t^2,\mu_t\right)$ under the risk-neutral probability Q. Define the conditional characteristic function of $\left(v_{t+\Delta}^2,\mu_{t+\Delta}\right)$ given $\left(v_t^2,\mu_t\right)$ under Q,

$$\bar{c}_\delta\left(t,v_t^2,\mu_t;\vartheta_1,\vartheta_2\right)=\mathbb{E}_t\left(e^{\mathtt{i}\vartheta_1 v_{t+\delta}^2+\mathtt{i}\vartheta_2\mu_{t+\Delta}}\right)=e^{\varsigma_1(t,\delta,\vartheta_1,\vartheta_2)+\varsigma_2(t,\delta,\vartheta_1,\vartheta_2)v_t^2+\varsigma_3(t,\delta,\vartheta_1,\vartheta_2)\mu_t}, \tag{B.13}$$

where the three functions $\varsigma_j\left(t,\Delta,\vartheta_1,\vartheta_2\right)$ satisfy

$$\left\{\begin{array}{l}
0=\dot{\varsigma}_1\left(\tau,\cdot\right)+\kappa_\mu m\varsigma_3\left(\tau,\cdot\right) \\
0=\dot{\varsigma}_2\left(\tau,\cdot\right)-\kappa_v\varsigma_2\left(\tau,\cdot\right)+\frac{1}{2}\xi^2\varsigma_2^2\left(\tau,\cdot\right) \\
0=\dot{\varsigma}_3\left(\tau,\cdot\right)+\kappa_v\varsigma_2\left(\tau,\cdot\right)-\kappa_\mu\varsigma_3\left(\tau,\cdot\right)+\frac{1}{2}\gamma^2\varsigma_3^2\left(\tau,\cdot\right)
\end{array}\right.$$

subject to the boundary conditions

$$\varsigma_1\left(t+\delta,\delta;\vartheta_1,\vartheta_2\right)=0\quad\text{and}\quad\varsigma_{j+1}\left(t+\delta,\delta;\vartheta_1,\vartheta_2\right)=\mathtt{i}\vartheta_j,\quad j=1,2.$$

The transition density $f_\Delta^F\left(v_{t+\Delta}^2,\mu_{t+\Delta}\big|\,v_t^2,\mu_t\right)$ is obtained as the Fourier's inverse transform of $\bar{c}_\delta\left(t,v_t^2,\mu_t;\vartheta_1,\vartheta_2\right)$ in (B.13), viz

$$f_\delta\left(v_{t+\Delta}^2,\mu_{t+\Delta}\big|\,v_t^2,\mu_t\right)=\frac{1}{\left(2\pi\right)^2}\int_{-\infty}^{\infty}\int_{-\infty}^{\infty}e^{-\mathtt{i}\vartheta_1 v_{t+\delta}^2-\mathtt{i}\vartheta_1\mu_{t+\delta}}\bar{c}_\delta\left(t,v_t^2,\mu_t;\vartheta_1,\vartheta_2\right)d\vartheta_1 d\vartheta_2. \tag{B.14}$$

Next, we determine $f_\Delta^F\left(x,y|\,v_t^2,\mu_t\right)$ in (24)—the transition density of $\left(v_{t+\Delta}^2,\mu_{t+\Delta}\right)$ given $\left(v_t^2,\mu_t\right)$ under the forward probability $Q_{t+\Delta}$. The conditional characteristic function under $Q_{t+\Delta}$ is defined as

$$\bar{c}_\Delta^F\left(t,v_t^2,\mu_t;\vartheta_1,\vartheta_2\right)=\mathbb{E}_t^{Q_{t+\Delta}}\left(e^{\mathtt{i}\vartheta_1 v_{t+\Delta}^2+\mathtt{i}\vartheta_2\mu_{t+\Delta}}\right)=e^{\zeta_1(t,\Delta,\vartheta_1,\vartheta_2)+\zeta_2(t,\Delta,\vartheta_1,\vartheta_2)v_t^2+\zeta_3(t,\Delta,\vartheta_1,\vartheta_2)\mu_t}, \tag{B.15}$$

for three functions $\zeta_j\left(t,\Delta,\vartheta_1,\vartheta_2\right)$ to be determined below (see Eqs. (B.16)-(B.17)). By the last two equations of (12), we know that $\left(v_t^2,\mu_t\right)$ satisfy

$$\left\{\begin{array}{rcl}
dv_\tau^2 &=& \left(\kappa_v\mu_\tau-G_{t+\Delta}\left(\tau\right)v_\tau^2\right)d\tau+\xi v_\tau\left(\rho dW_{1\tau}^{t+\Delta}+\sqrt{1-\rho^2}dW_{2\tau}^{t+\Delta}\right) \\
d\mu_\tau &=& \left(\kappa_\mu m-H_{t+\Delta}\left(\tau\right)\mu_\tau\right)d\tau+\gamma\sqrt{\mu_\tau}dW_{3\tau}^{t+\Delta}
\end{array}\right.$$

where $W_{j\tau}^{t+\Delta}$ are standard Brownian motions under $Q_{t+\Delta}$, and the two functions $G_X\left(\tau\right)$ and $H_X\left(\tau\right)$ are defined in Eqs. (14). By standard arguments, similar to those leading to Eqs. (A.30) in the two-factor case, we find

that the three functions $\zeta_j(t,\Delta,\vartheta)$ in Eq. (B.15) satisfy, for $\tau\in[t,t+\Delta)$,

$$\begin{cases} 0=\dot{\zeta}_1(\tau,\cdot)+\kappa_\mu m\zeta_3(\tau,\cdot) \\ 0=\dot{\zeta}_2(\tau,\cdot)-G_{t+\Delta}(\tau)\zeta_2(\tau,\cdot)+\frac{1}{2}\xi^2\zeta_2^2(\tau,\cdot) \\ 0=\dot{\zeta}_3(\tau,\cdot)+\kappa_v\zeta_2(\tau,\cdot)-H_{t+\Delta}(\tau)\zeta_3(\tau,\cdot)+\frac{1}{2}\gamma^2\zeta_3^2(\tau,\cdot) \end{cases} \tag{B.16}$$

subject to the boundary conditions

$$\zeta_1(t+\Delta,\Delta;\vartheta_1,\vartheta_2)=0 \quad \text{and} \quad \zeta_{j+1}(t+\Delta,\Delta;\vartheta_1,\vartheta_2)=\mathtt{i}\vartheta_j, \quad j=1,2. \tag{B.17}$$

The transition density $f_\Delta^F\left(v_{t+\Delta}^2,\mu_{t+\Delta}\middle|\, v_t^2,\mu_t\right)$ is the Fourier's inverse transform of $\bar{c}_\Delta^F\left(t,v_t^2,\mu_t;\vartheta_1,\vartheta_2\right)$ in Eq. (B.15):

$$f_\Delta^F\left(v_{t+\Delta}^2,\mu_{t+\Delta}\middle|\, v_t^2,\mu_t\right)=\frac{1}{(2\pi)^2}\int_{-\infty}^{\infty}\int_{-\infty}^{\infty}e^{-\mathtt{i}\vartheta_1 v_{t+\Delta}^2-\mathtt{i}\vartheta_1\mu_{t+\Delta}}\bar{c}_\Delta^F\left(t,v_t^2,\mu_t;\vartheta_1,\vartheta_2\right)d\vartheta_1 d\vartheta_2. \tag{B.19}$$

Appendix C: Details regarding model calibration

C.1. Futures

The model calibration relies on TY option implied volatilities. We use these implied volatilities to implement nonparametric estimates of hypothetical TYVIX future values, the benchmark in our optimization procedures. Accordingly, firstly, we provide a comprehensive derivation of these benchmarks as well as the approximations involved into them; and secondly, we provide details regarding the calibration of our model.

Non-parametric estimates of futures values. We derive non-parametric benchmarks for our model-based TYVIX futures values that rely on calendar spreads, which are originally proposed by Carr and Wu (2006) and Dupire (2006) in the equity case. Consider a generic Δ-forward looking variance gauge (e.g., $\Delta=\frac{1}{12}$) for a generic risk:

$$\mathrm{Vx}_{t,\Delta}^2\equiv\mathbb{E}_t^*\left(\frac{1}{\Delta}\int_t^{t+\Delta}\sigma_\tau^2 d\tau\right),$$

where σ_τ^2 denotes the instantaneous variance of this risk, and the conditional expectation $\mathbb{E}_t^*$ is taken under some numéraire probability (Mele and Obayashi, 2015).

Consider the price of a future on Vx expiring at $t+\delta$:

$$F_{t,t+\delta}\equiv\mathbb{E}_t\left(\mathrm{Vx}_{t+\delta,\Delta}\right),$$

where now $\mathbb{E}_t$ denotes the expectation under the risk-neutral probability. Let us, first, determine the expected squared Vx at $t+\delta$,

$$\begin{aligned}\mathbb{E}_t\left(\mathrm{Vx}_{t+\delta,\Delta}^2\right)&=\mathbb{E}_t\left(\mathbb{E}_{t+\delta}^*\left(\frac{1}{\Delta}\int_{t+\delta}^{t+\delta+\Delta}\sigma_\tau^2 d\tau\right)\right)\\&\approx\mathbb{E}_t\left(\mathbb{E}_{t+\delta}\left(\frac{1}{\Delta}\int_{t+\delta}^{t+\delta+\Delta}\sigma_\tau^2 d\tau\right)\right)\\&=\mathbb{E}_t\left(\frac{1}{\Delta}\int_{t+\delta}^{t+\delta+\Delta}\sigma_\tau^2 d\tau\right)\end{aligned}$$

$$= \frac{1}{\Delta}\mathbb{E}_t\left(\int_t^{t+\delta+\Delta}\sigma_\tau^2 d\tau - \int_t^{t+\delta}\sigma_\tau^2 d\tau\right)$$
$$= \frac{\delta+\Delta}{\Delta}\mathrm{Vx}^2_{t,\delta+\Delta} - \frac{\delta}{\Delta}\mathrm{Vx}^2_{t,\delta}. \tag{C.1}$$

The second line is only an approximation because the risk-neutral probability and the numéraire probability are generically not the same. For example, in our context, the numéraire probability is the forward probability.

Next, fix $\Delta = \frac{1}{12}$, and set the futures month maturity equal to $\delta = q\Delta$, for integer q, such that the approximation in (C.1) is:

$$\mathbb{E}_t\left(\mathrm{Vx}^2_{t+q\Delta,\Delta}\right) \approx (q+1)\,\mathrm{Vx}^2_{t,(q+1)\Delta} - q\mathrm{Vx}^2_{t,q\Delta}. \tag{C.2}$$

Note that $F_{t+q\Delta,t+q\Delta} = \mathrm{Vx}_{t+q\Delta,\Delta}$, such that:

$$\begin{aligned}\mathbb{E}_t\left(F_{t+q\Delta,t+q\Delta}\right)^2 &= \mathbb{E}_t\left(\mathrm{Vx}^2_{t+q\Delta,\Delta}\right) - var_t\left(F_{t+q\Delta,t+q\Delta}\right)\\ &\approx (q+1)\,\mathrm{Vx}^2_{t,(q+1)\Delta} - q\mathrm{Vx}^2_{t,q\Delta} - var_t\left(F_{t+q\Delta,t+q\Delta}\right),\end{aligned}$$

where the second line follows by the approximation in (C.2). Therefore, we have the following approximations:

$$\begin{aligned}F_{t,t+q\Delta} &= \mathbb{E}_t\left(F_{t+q\Delta,t+q\Delta}\right)\\ &\approx \sqrt{(q+1)\,\mathrm{Vx}^2_{t,(q+1)\Delta} - q\mathrm{Vx}^2_{t,q\Delta} - var_t\left(F_{t+q\Delta,t+q\Delta}\right)}\\ &\approx \sqrt{(q+1)\,\mathrm{Vx}^2_{t,(q+1)\Delta} - q\mathrm{Vx}^2_{t,q\Delta}}.\end{aligned} \tag{C.3}$$

In the calibration, we use the CBOT 10-Year Treasury Note option ATM implied volatility at day n for maturity δ, $\mathrm{atm}_n(\delta)$, as a proxy for $\mathrm{Vx}_{n,\delta}$, to calculate the previous expression and use it as a non-parametric estimate of hypothetical TYVIX future values; see Eq. (C.6) below.

Calibration and other optimization procedures. Consider the following estimate of the basis point variance v_n^2 of the short-term rate on each day n in our sample:

$$\hat{\sigma}_n^2 \equiv \frac{252}{30}\sum_{i=1}^{30}\left(r_{n-i+1} - r_{n-i}\right)^2,$$

where r_n is the 3-month Treasury Bill rate as of day n. We calibrate κ_v in (8) while assuming $\hat{\sigma}_n^2$ has the same autocovariance function as the true basis point variance, thereby estimating κ_v while fitting an autoregressive model to the $\hat{\sigma}_n^2$ series. Likewise, we calibrate the volatility of variance parameter ξ in (8) to match the average volatility of changes in the basis point variance, $\sqrt{\frac{\Delta^{-1}\mathrm{var}(\Delta\hat{\sigma}_n^2)}{\mathrm{avg}(\hat{\sigma}_n^2)}}$, where $\Delta^{-1} = \frac{1}{252}$, and $\mathrm{var}(\Delta\hat{\sigma}_n^2)$ and $\mathrm{avg}(\hat{\sigma}_n^2)$ denote the sample variance of the daily changes in $\hat{\sigma}_n^2$ and the sample average of $\hat{\sigma}_n^2$, respectively. As explained in the main text, κ_μ and γ are calibrated in the same way, based on model-implied values of μ (see Steps 1 to 3 below).

To estimate TYVIX future values, we proceed through four steps. In the first three steps, we calibrate the two-factor model in Appendix A and obtain model-implied values of the long-term basis point parameter μ for each day of the sample. We utilize these values to calibrate the parameters κ_μ, m and γ. In the fourth and last step, we use all the parameter estimates in Table 1 and re-calibrate the full three-factor model to estimate TYVIX futures values. In the following, V_n denotes the value of the TYVIX index as of day n, and N is the sample size.

Step 1 Fix κ_r at some value $\hat{\kappa}_r$.

Step 2 For each day n, calibrate μ in the two-factor model so as to fit the two-month term-structure of a

non-parametric estimate of TYVIX futures based on Eq. (C.3):

$$\hat{\mu}_{\text{ini},n}\left(\hat{\kappa}_r\right) \equiv \arg\min_{\mu} \sum_{j=1}^{2} \left(\hat{\mathcal{F}}(\mathsf{Y}^{\$}_{n,\mathbb{T}}, \hat{v}^2_{\text{ini},n}; n+\delta_j, T, S, \mathbb{T}; \hat{\kappa}_r) - \mathcal{F}^{\$}_n\left(\delta_j\right) \right)^2, \tag{C.4}$$

under the constraint that

$$\hat{v}^2_{\text{ini},n} = \hat{v}^2_{\text{ini},n}\left(\mu\right) \equiv \frac{V_n^2 - \kappa_v \mu \mathcal{A}_1(\mathsf{Y}^{\$}_{n,\mathbb{T}}, T, S, \mathbb{T})}{\mathcal{A}_2(\mathsf{Y}^{\$}_{n,\mathbb{T}}, T, S, \mathbb{T})}, \tag{C.5}$$

where $\hat{\mathcal{F}}(\mathsf{Y}^{\$}_{n,\mathbb{T}}, \hat{v}^2_{\text{ini},n}; n+\delta_j, T, S, \mathbb{T}; \hat{\kappa}_r)$ is $\hat{\mathcal{F}}\left(\cdot\right)$ in Eq. (A.27) when the parameter $\kappa_r = \hat{\kappa}_r$, and

$$\mathcal{F}^{\$}_n\left(\delta_j\right) = \sqrt{\left(\delta_j + 1\right) \cdot \text{atm}^2_n\left(\delta_j + 1\right) - \delta_j \cdot \text{atm}^2_n\left(\delta_j\right)} \tag{C.6}$$

is a non-parametric estimate of the future value at day n, expiring at day $n+\delta_j$, with δ_j equal to one and two months. The constraint (C.5) guarantees that the two-factor model prediction (Eq. (A.26)) exactly matches the TYVIX. The rationale underlying the non-parametric estimate $\mathcal{F}^{\$}_n\left(\delta_j\right)$ relies on the derivations leading to Eq. (C.3). The next step describes how values $\hat{\kappa}_r$ in Step 1 are updated given the calibration of μ_n in this step.

Step 3 Iterate on $\hat{\kappa}_r$ and the calibrated values $(\hat{\mu}_n)_{n=1}^N$ in Steps 1 and 2, to ensure that

$$\hat{\kappa}_r\left(\hat{\mu}_n\right) \equiv \arg\min_{\kappa_r} \left(\text{avg}\left(\hat{v}^2_{\text{ini},n}\left(\hat{\mu}_{\text{ini},n}\left(\kappa_r\right)\right)\right) - \text{avg}\left(\hat{\sigma}^2_n\right)\right)^2.$$

Step 4 Estimate κ_μ by fitting an autoregressive model to the calibrated values of $(\hat{\mu}_{\text{ini},n})_{n=1}^N$ obtained in the previous steps, and set $m = \text{avg}\left(\hat{\mu}_{\text{ini},n}\right)$ and $\gamma = \sqrt{\frac{\Delta^{-1}\text{var}(\Delta\hat{\mu}_{\text{ini},n})}{\text{avg}(\hat{\mu}_{\text{ini},n})}}$. Revise the estimates of the series $(\hat{v}^2_{\text{ini},n}, \hat{\mu}_{\text{ini},n})_{n=1}^N$ while minimizing the distance of model-implied TYVIX futures to their non-parametric counterparts:

$$\hat{\mu}_n \equiv \arg\min_{\mu_n} \sum_{j=1}^{2} \left(\hat{\mathcal{F}}(\mathsf{Y}^{\$}_{n,\mathbb{T}}, \hat{v}^2_n, \mu_n; n+\delta_j, T, S, \mathbb{T}; \hat{\kappa}_r) - \mathcal{F}^{\$}_n\left(\delta_j\right) \right)^2,$$

under the constraint that the model-implied realized variance makes the three-factor model-implied TYVIX equal to TYVIX for each day, relying on Eq. (19),

$$\hat{v}^2_n = \frac{V_n^2 - \kappa_\mu m \mathcal{B}_1(\mathsf{Y}^{\$}_{n,\mathbb{T}}, T, S, \mathbb{T}) - \mathcal{B}_3(\mathsf{Y}^{\$}_{n,\mathbb{T}}, T, S, \mathbb{T})\hat{\mu}_n}{\mathcal{B}_2(\mathsf{Y}^{\$}_{n,\mathbb{T}}, T, S, \mathbb{T})}, \tag{C.7}$$

and where $\hat{\mathcal{F}}(\mathsf{Y}^{\$}_{t,\mathbb{T}}, v^2_t, \mu_t; t+\delta, T, S, \mathbb{T})$ is $\hat{\mathcal{F}}\left(\cdot\right)$ in Eq. (22).

C.2. Options

We approximate $\hat{\mathcal{C}}^f_t\left(t, v^2_t, \mu_t; t+\Delta, K, T, S, \mathbb{T}\right)$ in Eq. (31) as follows. Given the history of calibrated futures values obtained in Section 5.2.1, we perform a non-parametric regression of these calibrated values on to the model-implied v^2_t and μ_t and $\mathcal{B}_{jt} \equiv \mathcal{B}_j(\mathsf{Y}^{\$}_{t,\mathbb{T}}, T, S, \mathbb{T})$, so as to learn about the functional relation linking these variables to the calibrated one. This functional relation is model-based, thereby leading to small error margins. Denote with $\hat{\mathbb{F}}\left(v^2_t, \mu_t, \mathcal{B}_{1t}, \mathcal{B}_{2t}, \mathcal{B}_{3t}; t+\delta, T, S, \mathbb{T}\right)$ the predictive part of this non-parametric regression. We approximate the price $\hat{\mathcal{C}}^f_t$ in Eq. (31) using this estimate, and freezing $\mathsf{Y}_{T,\mathbb{T}}$ at $\mathsf{Y}^{\$}_{t,\mathbb{T}}$, thereby freezing $\mathcal{B}_{jT}$ at

$\mathcal{B}_{jt}$:

$$\begin{aligned}
&\hat{\mathbb{C}}^f(\mathsf{Y}^{\$}_{t,\mathbb{T}}, v_t^2, \mu_t; t+\Delta, K, T, S, \mathbb{T}) \\
&\equiv P_t(T) \iint \left(\hat{\mathbb{F}}(x, y, \mathcal{B}_{1t}, \mathcal{B}_{2t}, \mathcal{B}_{3t}; T+\delta, T, S, \mathbb{T}) - K\right)^+ f_\Delta^F\left(x, y \middle| v_t^2, \mu_t\right) dxdy. \qquad \text{(C.8)}
\end{aligned}$$

Note, now, that as a result of freezing $\mathsf{Y}^{\$}_{T,\mathbb{T}}$ to $\mathsf{Y}^{\$}_{t,\mathbb{T}}$, $\hat{\mathbb{C}}^f$ in (C.8) now depends on $\mathsf{Y}^{\$}_{t,\mathbb{T}}$, whereas $\hat{\mathcal{C}}_t^f$ in (31) depends on a generic t.

References

Bakshi, Gurdip and Dilip Madan, 2000. "Spanning and Derivative Security Evaluation." *Journal of Financial Economics* 55, 205-238.

Bates, David S., 2012. "U.S. Stock Market Crash Risk, 1926-2010." *Journal of Financial Economics* 105, 229-259.

Bansal, Ravi and Amir Yaron, 2004 "Risks for the Long-Run: A Potential Resolution of Asset Pricing Puzzles." *Journal of Finance* 59, 1481-1509.

Britten-Jones, Mark and Anthony Neuberger, 2000. "Option Prices, Implied Price Processes and Stochastic Volatility." *Journal of Finance* 55, 839-866.

Brigo, Damiano and Fabio Mercurio, 2006. *Interest Rate Models—Theory and Practice, with Smile, Inflation and Credit*. Springer Verlag, Springer Finance Series, Heidelberg (2nd Edition).

Carr, Peter and Dilip Madan, 2001. "Optimal Positioning in Derivative Securities." *Quantitative Finance* 1, 19-37.

Carr, Peter and Liuren Wu, 2006. "A Tale of Two Indices." *The Journal of Derivatives* 16, 13-29.

Collin-Dusfresne, Pierre and Robert S. Goldstein, 2002. "Do Bonds Span the Fixed-Income Markets? Theory and Evidence for Unspanned Stochastic Volatility." *Journal of Finance* 57, 1685–1730.

Demeterfi, Kresimir, Emanuel Derman, Michael Kamal, and Joseph Zou, 1999,a. "A Guide to Variance Swaps." *Risk* 12(6) June, 54-59.

Demeterfi, Kresimir, Emanuel Derman, Michael Kamal, and Joseph Zou, 1999,b. "A Guide to Volatility and Variance Swaps." *The Journal of Derivatives* 6(4) Summer, 9-32.

Duffee, Gregory, 2002. "Term Premia and Interest Rate Forecasts in Affine Models." *Journal of Finance* 57, 405-443.

Duffie, D., D. Filipović and W. Schachermayer, 2003. "Affine Processes and Applications in Finance." *The Annals of Applied Probability* 13, 984-1053.

Dupire, Bruno, 2006. "Model Free Results on Volatility Derivatives." Bloomberg NY, Unpublished manuscript.

Egloff, Daniel, Markus Leippold, and Liuren Wu, 2010. "Valuation and Optimal Investing in Variance Swaps." *Journal of Financial and Quantitative Analysis* 45, 1279-1310.

Engle, Robert F., 2004. "Nobel Lecture: Risk and Volatility: Econometric Models and Financial Practice." *American Economic Review* 94, 405-420.

Heston, Steven L., 1993. "A Closed Form Solution for Options with Stochastic Volatility with Applications to Bond and Currency Options." *Review of Financial Studies* 6, 327-344.

Ho, Thomas, S.Y. and Sang B. Lee, 1986. "Term Structure Movements and the Pricing of Interest Rate Contingent Claims." *Journal of Finance* 41, 1011-1029.

Mele, Antonio, 2007. "Asymmetric Stock Market Volatility and the Cyclical Behavior of Expected Returns." *Journal of Financial Economics* 86, 446-478.

Mele, Antonio, 2019. *Financial Economics*. MIT Press, forthcoming.

Mele, Antonio and Yoshiki Obayashi, 2015. *The Price of Fixed Income Market Volatility*. Springer Verlag, Springer Finance Series. New York.

Mele, Antonio and Yoshiki Obayashi, 2016. "Interest Rate Derivatives and Volatility." In: Pietro Veronesi (Editor), *The Handbook of Fixed Income Securities*, John Wiley and Sons (Handbook Series in Financial Engineering and Econometrics), Chapter 20, 767-838.

Mencía, Javier and Enrique Sentana, 2013. "Valuation of VIX Derivatives." *Journal of Financial Economics* 108, 367-391.

Rebonato, Riccardo, 1998. *Interest Rate Option Models*. John Wiley, Chichester (2nd Edition).